MoS_2 Doped TiO_2 Nanomaterial and the Enhancement of Photocatalytic Properties for Solar Disinfection

by

Timothy McColgan

A thesis submitted in partial fulfillment of the requirements
for the degree of Master of Science
Department of Environmental Science, Policy and Geography
College of Arts and Sciences
University of South Florida St. Petersburg

Major Professor: Henry Alegria, Ph.D.
Madhu Pandey, Ph.D.
Foday Jaward, Ph. D.

Defense Date: March 20th 2018

Keywords: molybdenum, titanium, biological decontamination, Sol-Gel synthesis, hydrolysis

Dedication

Mom and Dad-- thanks for tirelessly providing me encouragement to achieve and prepare for the future.

Acknowledgements

I'd like to extend my gratitude to Dr. Pandey for providing me with her time, dedication, and guidance. This project would not have happened without her. To Dr. Ram and his research assistants, Srikanth Gunti and Turk Alamro, thank you sincerely for the research project idea and the analytical assistance. I'd like to give a special thanks to Dr. Alegria, for taking on another project given his busy schedule. Finally, I'd like to thank the University of South Florida St. Petersburg for providing me the education necessary to complete this research project and two years of graduate assistantships.

Table of Contents

List of Tables

List of Figures

Abstract

This research project focused on the synthesis, characterization, and environmental application of a photocatalytic nanomaterial composed of molybdenum (IV) disulfide [MOS_2] doped titanium dioxide [TiO_2]. Extensive research has been conducted on the electronic uses of nanocrystalline MoS_2 as a phototransistor and absorptive species (Yin et al., 2012), as well as the photocatalytic effects of TiO_2 (Diebold, 2003). Research has also been performed into the generation of oxidizers from TiO_2 nanocomposites (Zhang et al., 2015), but as of yet no research has been conducted on a practical application of this material. This project fills that void by evaluating its effectiveness while integrated into a solar disinfection [SODIS] platform, which has extensive humanitarian applications. Solar disinfection is the chief disinfection method recommended by the World Health Organization for developing countries (Clasen, 2008).

This project utilized the Sol-gel method to create varying concentrations of MoS_2-TiO_2 nanocomposite, followed by characterization using SEM (scanning electron microscopy), X-ray diffraction, FTIR spectrophotometer analysis, and solid state UV-Visible analysis. It was successfully demonstrated that a synthesis of these two materials is possible at a variety of ratios, but that a blend of 5% MoS_2-95% TiO_2 enhanced the photocatalytic properties of TiO_2 most optimally when integrated into the SODIS platform. Doping with low concentrations of MoS_2 enhanced the absorption of light by TiO_2 into the visible spectrum and increased its absorbance into the UVB/UVA range, without inhibiting its inherent oxidative properties significantly. This enhancement

resulted in a reduction to the time required for full elimination of deleterious Escherichia Coli [E. coli] from potable water within the SODIS platform from 150 minutes to 120 minutes, compared to pure TiO_2 nanomaterial. It was also demonstrated that the other blends of MoS_2 doped TiO_2 possessed equivalent photocatalytic properties compared to that of pure TiO_2 (Yin et al., 2012). If properly employed, these nanocomposites could serve as an effective addition to the SODIS platform.

Chapter 1: Introduction

Alongside air and food, potable water is the most essential substance for sustaining human life. All societies revolve around harvests for cooking, drinking, and sanitary purposes. Water is held in spiritual regard cross-culturally; it is integral to Christian, Hindu, and Muslim ritual and worship. This affirms water's role as a creator, giver of life and of fertility. Yet for as long as water has been worshipped, humans have also worked to mitigate water's role as a media for spreading malady and death. Thus, water pollution abatement is arguably one of the most critical goals for environmental sciences. Methods for the disinfection and remediation of debilitating water contaminants have been implemented for thousands of years, long before the principles of these phenomena were understood. Although it is hypothesized that prehistoric humans utilized methods for the purification of water, the first definitive proof of disinfection implementation dates back over 4000 years to early Sanskrit medical texts. Documented methods include sand filtration, clarification, exposure to ultraviolet radiation and boiling. By 2000 B.C., the Greeks pioneered a method for the disinfection of water by exposing it to direct sunlight and oxygen (EPA, 2000). Although no longer employed in countries with advanced treatment facilities, refinement of the Greek method has pushed the relevancy of solar disinfection to modern times in countries where infrastructure is lacking and contamination of drinking water by fecal-related bacteria occurs routinely.

Currently, solar disinfection (SODIS) is recommended as a primary purification process by the World Health Organization in conjunction with physical filtration

methods. SODIS eliminates biological pathogens including bacteria, protozoans, and viruses through the combination of both light and heat. Proper employment of the SODIS process can greatly reduce mortality in children, the population most at risk from gastrointestinal diseases caused by waterborne Salmonella, Shigella, Escherichia Coli, and Vibrio Cholerae (Meierhofer et al., 2002).

SODIS is non-electrical and relies on the generation of ozone (O_3) when the UV-A spectrum (320-400 nm) of sunlight reacts with aqueous Oxygen (O_2) (Meierhofer et al. 2002). Dissolved O_2 molecules are split, forming oxygen free radicals (O^*) which bond onto a nearby diatomic oxygen molecule, as shown in Figure 1. Ozone molecules have a high oxidation potential, making them deadly to waterborne microorganisms (Lonnen et al., 2005). SODIS is applicable to international communities because it requires only simple materials, is portable, and can be employed at a household level (Meierhofer et al., 2002). Although effective in optimal conditions, the SODIS method suffers from long purification times (up to six hours), the necessity of unabated exposure to direct sunlight, and the potential of coliform regrowth during storage (Gelover et al., 2006).

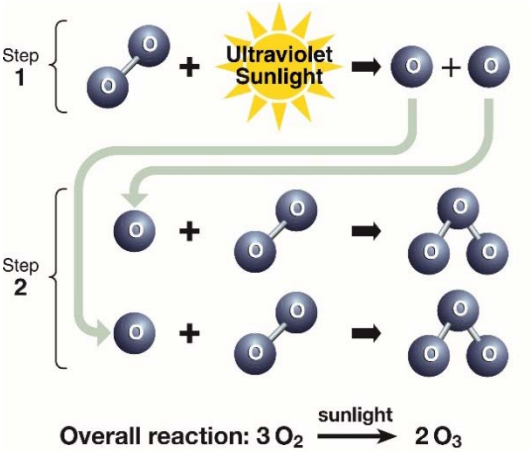

Figure 1: Reaction mechanism demonstrating formation of ozone (Fahey et al., 2011).

Improvements to the SODIS method have naturally led to the introduction of photocatalysts in the treatment process. Photocatalysts are materials which can speed the oxidation of bacteria through the generation of hydroxyl radicals (OH^-) and oxide ions (O_2) in drinking water, leading to a direct reduction in the decontamination time required by the SODIS process and to preventing the regrowth of fecal coliform after treatment (Gelover et al., 2006). The properties of the first nonelectrical photocatalyst, TiO_2, were discovered by Kenichi Honda and Akira Fujishima in 1972. Their research demonstrated that when TiO_2 was exposed to intense light, the generation of hydrogen gas was observed (Fujishima et al., 1972). This is because TiO_2 possesses the properties of a semiconductor. Semiconductors differ from metals and insulators due to their narrow band gap; band gap is a measurement of the energy required to excite a semiconductor and move an electron from bands closest to the nucleus (valence bands) to bands further from the nucleus (conduction bands) (Asahi, 2001). Metals have no band gap, which makes them excellent conductors of electricity as electrons move uninhibited from the valence to conduction bands. This differs from insulators, which have a band gap too large for the transmission of electrons. When electron movement occurs between the band gaps in a semiconducting material, a positive hole (h^+) is formed in the valence band; this hole is responsible for the generation of hydrogen gas initially observed by Honda and Fujishima. H_2O molecules undergo hydrolysis at the h^+ site into H+ and OH- (Asahi, 2001). In turn, the electron released into the conduction band reacts at the surface of the semiconductor with oxygen to form the oxide ion (O_2^-). Both OH^- and O_2^- are powerful oxidizers that when dissolved within a solution can decrease the time required for disinfection. This is a decrease in time from over 80 minutes utilizing SODIS to 30

minutes for the complete elimination of fecal coliforms utilizing SODIS bottles coated with pure TiO_2 (Gelover et al., 2006).

The band gap of TiO_2 is 3.19 eV (electron volts) (Asahi, 2001), and is calculated by the following formula:

$$E(eV) = \frac{hc}{\lambda} = \frac{(4.135667516 \cdot 10^{-15}\ eV\,s)(299792458\ m/s)}{\lambda\ (nm)} = \frac{1239.84192\ eV \cdot nm}{\lambda\ (nm)}$$

where E (eV) is calculated by multiplying Planck's constant (h) by the speed of light (c) in a vacuum, and dividing it by the longest wavelength of light absorbed by the semiconductor (λ) causing photoexcitation. Due to the 3.19 eV band gap of TiO_2, only wavelengths shorter than 388 nm mediate this process (Carp et al., 2004). Thus, the utilization of pure TiO_2 for SODIS is limited by the availability of UV light, which comprises at most 3-5% of total sunlight hitting the earth due to filtration by the ozone layer (Emery, 2002). Concurrently, peak absorbance of UV light by TiO_2 occurs at 150 nm, 200 nm, and 240 nm, with significantly lower absorbance in the UVB/UVA range of 290-400 nm (Du and Li, 2010). The largest absorbance peaks of TiO_2 occur in the UVC wavelength, which is filtered completely from sunlight as it travels through the ozone layer and atmosphere (EPA, 2010).

Due to the absorbance limitations of TiO_2, a significant body of research has been generated around finding a way to reduce its band gap energy (Diebold, 2003). Reduction in band gap energy (eV) can extend the wavelength of light absorbed by TiO_2 into the visible range and can increase the intensity of absorbance in the UVB/UVA regions, which penetrate the ozone layer (Gunti et al., 2016). As a result, the photocatalytic potential of TiO_2 can be exponentially increased (Diebold, 2003). This reduction can be accomplished by doping the crystal lattice structure of a semiconductor; doping is a

process regularly employed in the creation of materials for use in diodes and transistors within the electronics manufacturing industry (Chen et al., 2010). Doping is done in order to increase the number of charge carriers in the crystal through the formation of semiconductor junctions, as well as lowering electrical resistance. An increase in charge carriers on the surface of crystal means that a greater number of positive holes (H^{+}) and released electrons can be generated, increasing oxidative potential (Chen et al., 2010). Doping of TiO_2 has been successfully tested with many metals and metal oxides, including Molybdenum (Diebold, 2003). Doping of TiO_2 to yield nanocomposites has been demonstrated to both extend and increase the intensity of absorbance of TiO_2 by reducing the band gap (Zhang et al., 2015). Utilizing TiO_2 doped with MoS_2 will likely increase the effectiveness of the SODIS process versus disinfection completed utilizing pure TiO_2. Until now, no research has been conducted utilizing a MoS_2-TiO_2 nanomaterial as a coating for SODIS bottles.

The research detailed herein has as its main goals: (1) synthesis, (2) characterization of MoS_2-TiO_2, and (3) testing the efficiency of this new nanomaterial as an inexpensive and expeditious way to disinfect water.

Chapter 2: Synthesis and Characterization of MoS_2-TiO_2 Complex

Synthesis

Synthesis of the MoS_2-TiO_2 complex was carried out using the Sol-Gel method (Hench and West, 1990). Sol-Gel is the most thoroughly researched process for the synthesis of materials consisting of nanoparticle TiO_2, as it is a reliable method for generating TiO_2 with a 3-dimensional, tightly -packed crystalline structure (Chen and Mao, 2007). Synthesis of the complex was carried out in batches with a desired yield of 40 grams per batch. For each batch, an anhydrous solution of 2-propanol and 100 mg of cetyltrimethylammonium bromide surfactant was prepared in a 2-liter flask. The amount of propanol required for each batch varied relative to the amount of titanium isopropoxide to be added during the synthesis, at a ratio of 5 ml 2-propanol to every 1 ml titanium isoproxide. Second, finely powdered MoS_2 was suspended in the solution with stirring. The amount of MoS_2 varied between batches, to achieve the correct ratio of MoS_2 to TiO_2 (Table 1). Finally, the desired amount of titanium isopropoxide (to achieve the desired ratio as per Table 1) was pipetted into the flask while placed in a sonication bath. Table 1 provides the exact measurements for each batch.

After adding the titanium isopropoxide, 750 mL of deionized water acidified to pH 2 with concentrated hydrochloric acid was added dropwise with vigorous stirring. During this stage, titanium isopropoxide is hydrolyzed into TiO_2, incorporating the suspended MoS_2 particles. The solution was allowed to stir for 24 hours. Later, the solution was washed with deionized water to fully remove surfactant and solvent, leaving

behind uncontaminated MoS_2-TiO_2 nanocomposite. Washing was carried out by transferring the original nanomaterial solution to a 4-liter flask. Deionized water was added to the nanomaterial solution to the 4-liter mark. This results in dilution of the 2-propanol solvent, and separates the cetyltrimethylammonium bromide, which remains suspended in the water after the nanomaterial has settled to the bottom. After settling, three liters of water was drawn off from above the product and discarded. This process was repeated a total of ten times to ensure that the surfactant and 2-propanol had been fully removed from the nanomaterial. After this process, the solution volume was reduced to 500 mL through settling of the product. 50 mL aliquots of nanomaterial suspension were transferred to evaporation dishes and dried in an oven at 100° C for 24 hours to anneal and fully dehydrate the powder. At this annealing temperature, it can be concluded that anatase TiO_2 is the primary crystalline shape generated, as annealing temperatures of 700° C are required to generate rutile TiO_2 in nano-powders (Hwu et al., 1997). Thus, XRD analytical measurements focus on anatase crystallography, rather than that of rutile TiO_2 (Luttrell et al., 2015). Each batch was then finely powdered for 20 minutes within a Fritsch Pulverisette ball mill using zirconium pellets to ensure finely milled particles optimized for photocatalytic experimentation.

Table 1: Data listing for the synthesis of MoS2-TiO2 batches.

Batch	**Theoretical Yield**	**Actual yield /Percent yield**	**Grams MoS_2 used**	**Grams TiO_2 produced**	**mL titanium isopropoxide used**	**mL 2-propanol used**	**mg surfactant used**
1.5% MoS_2 / 98.5% TiO_2	40 g	38.5 g/ 96%	0.6 g	39.4 g	146 mL	730 mL	100 mg
5% MoS_2 / 95% TiO_2	40 g	38.1 g/ 95%	2 g	38 g	141 mL	705 mL	100 mg
10% MoS_2 / 90% TiO_2	40 g	38.7 g/ 97%	4 g	36 g	133.5 mL	668 mL	100 mg

Characterization

X-ray Diffraction results:

XRD analysis is a useful tool for establishing the crystalline structure of a nanomaterial. It can also be used as an indicator of varying concentrations of a chemical between nanomaterial samples utilizing the same chemical precursors (Sakurai and Mizusawa, 2010). XRD analysis requires homogenized, finely powdered samples to ensure that the most accurate measurements are taken, thus highlighting the importance of extensive milling. Analysis of samples was performed at the Nanotechnology Research Education Center, USF Tampa. XRD analysis was run on the samples from 10° to 70 ° to illustrate any relevant constituents in a MoS_2-TiO_2 molecule. The machine used to run the samples was a PANalytical X'Pert^3 Powder XRD analyzer.

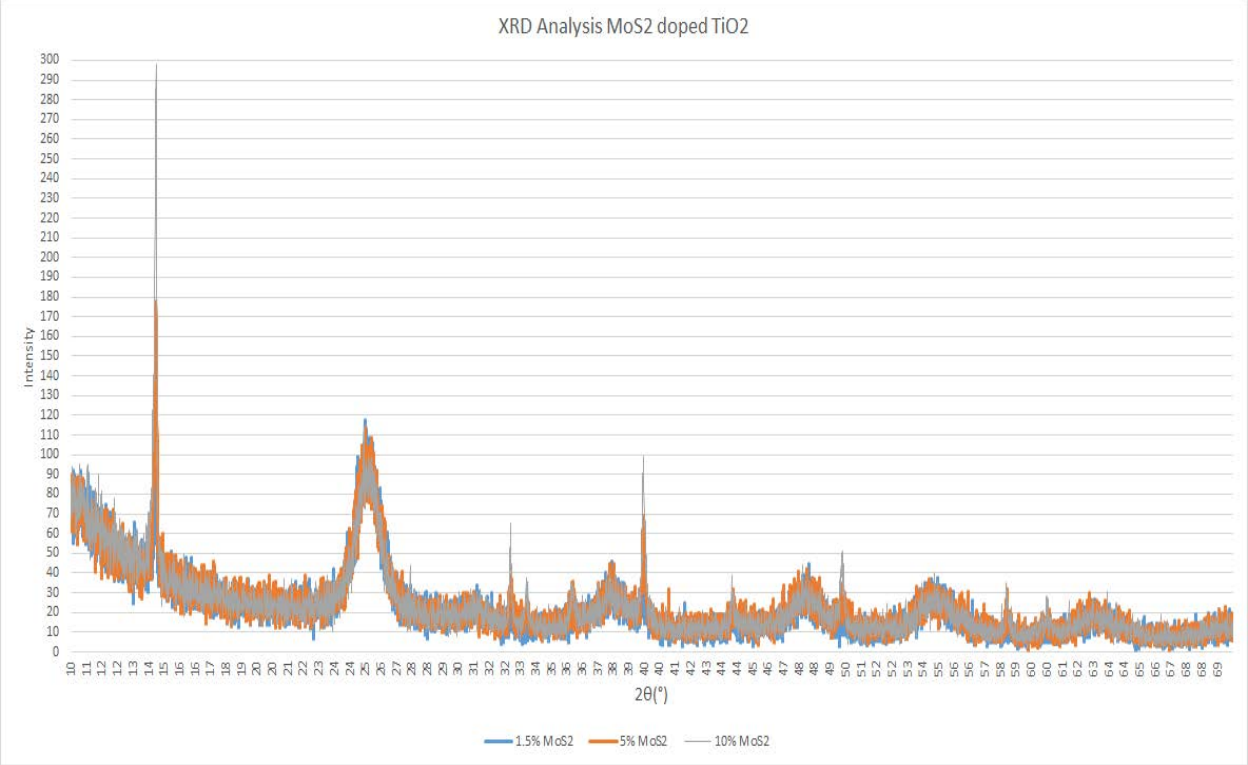

Figure 2: XRD overlay of the three concentrations of MoS_2 doped TiO_2

Figure 2 represents an overlay of XRD readings for the three concentrations of MoS_2-doped TiO_2. Peak intensity on the Y axis is indicative of a chemical's concentration within a sample, whereas the X axis represents the angle of diffraction during analysis. Chemicals have their own unique diffraction peak signature within an XRD readout due to their crystallography, with primary, secondary, and tertiary diffraction peaks. If synthesis was successful, analysis of this graph will reveal that the 1.5%, 5%, and 10% MoS_2-TiO_2 batches share the same peaks, but that peak intensity between the readings will vary due to differences in MoS_2 concentration relative to TiO_2 concentration. A key difference to note between samples is the concentration of dopant MoS_2, which should be illustrated by higher intensity peaks, characteristic of that chemical in the readout as its concentration increases. According to readings taken from XRD databases (Figures 3 and 4), peaks for MoS_2 are located at 14°, 32°, 40°, 49°, 58°, and 60° (Wildervanck and Jellinek, 1964), while key peaks for TiO_2 are located at 25°, 39°, 48°, 54°, 55°, 56°, 65°, and 70° (Sanchez et al., 1996). A key indicator of successful synthesis is indicated by increasing intensity of peaks 14°, 32°, 40°, and 49° as the concentration of MoS_2 increases. This will be coupled with a decrease in intensity of peaks at 25°, 39°, 48°, 55-56° as the concentration of TiO_2 in mixture decreases, relative to MoS_2.

Crystal size can be inferred from the width of a peak related to a particular chemical. According to Chen and Mao (2007), the width of a peak at half maximum is related to the particle size of a given crystalline compound and it also indicates the organizational structure of crystals within the nanomaterial. Peaks that are very thin indicate a well-organized crystal structure and larger crystals, while wider peaks are

associated with smaller crystals and mixed assemblages of molecules (Chen and Mao, 2007). Thus, another indicator of successful synthesis is indicated by wider peaks for TiO_2, as optimal particle size in the 5-20 micrometer range results in optimized photocatalytic activity (Wang et al., 1997).

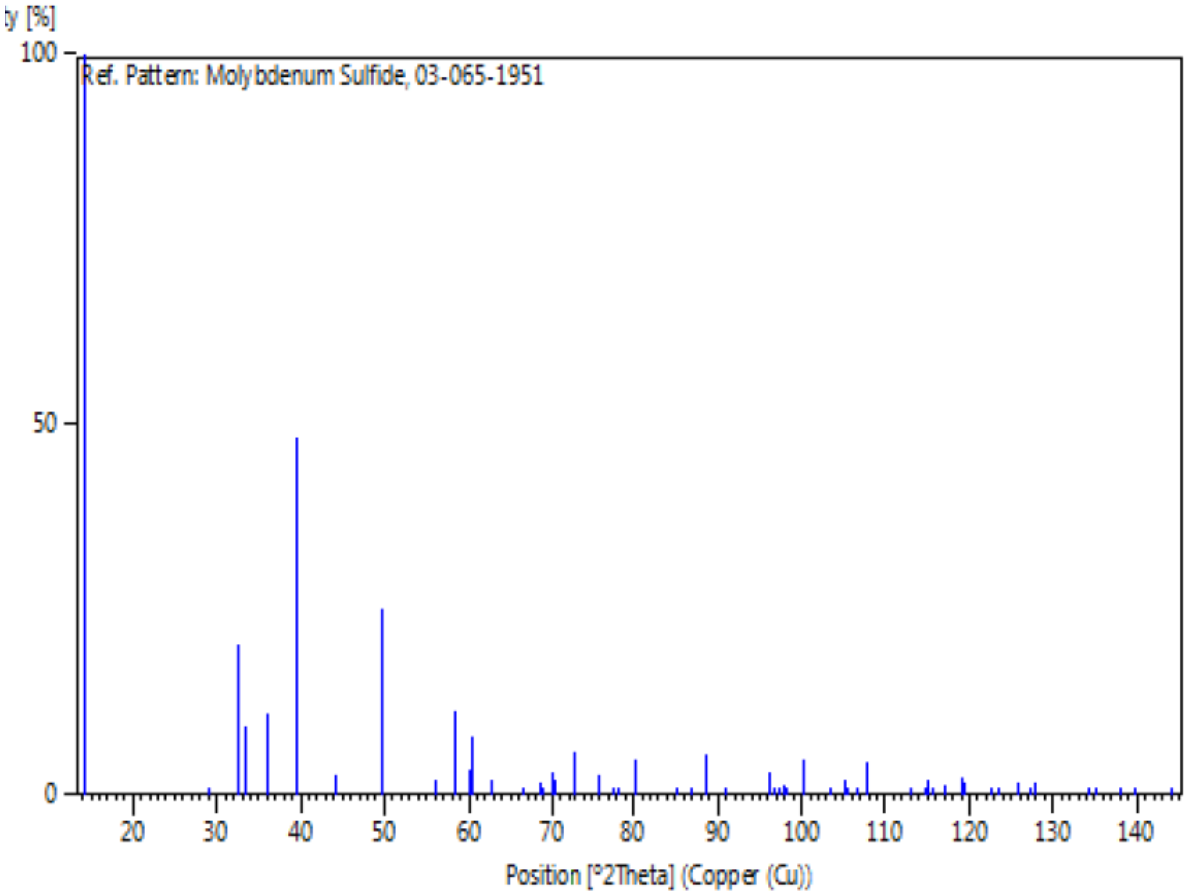

Figure 3: XRD readout of pure MoS_2 standard
Structure: J.C Wildervanck and F. Jellinek, Z. Anorg. Allg. Chem., 328, 309, (1964)

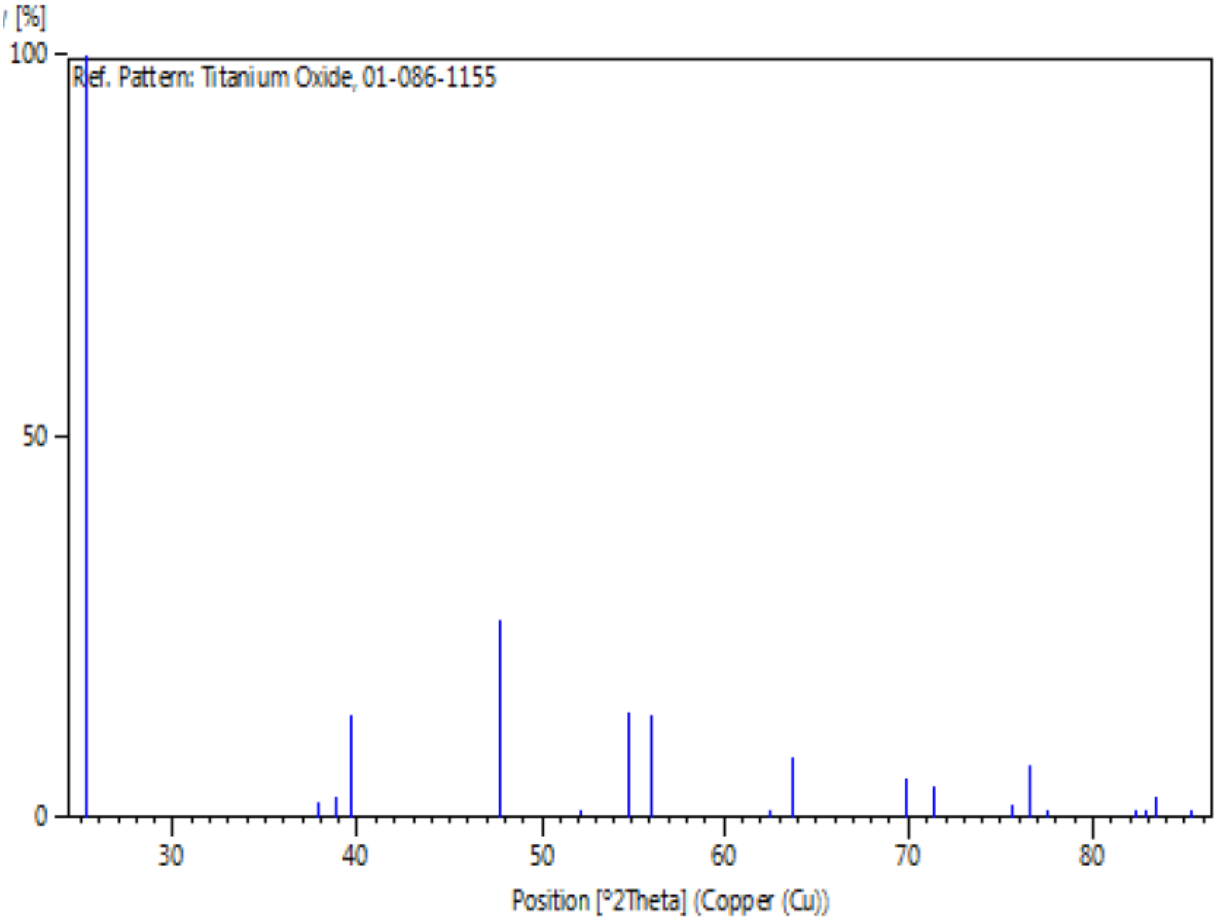

Figure 4: XRD readout of pure TiO_2 standard
Structure: Sanchez, E., Lopez, T., Gomez, R., Bokhimi, Morales, A., Novaro, O., J. Solid State Chem., 122, 309, (1996)

The analyzed sample of 1.5% MoS_2 doped TiO_2 showed peaks characteristic of both compounds (Fig. 5), which illustrates the absence of side products. The highest peak at 25° indicates the presence of TiO_2 as the primary peak. Importantly, the presence of a wide peak at this locus shows a small particle size for anatase TiO_2 (Chen and Mao, 2007). This peak had an intensity of nearly 120, the highest peak at 25° for all sample batches. This is a key property of the 1.5% batch, as it is the only batch synthesized where TiO_2 has a higher intensity than its MoS_2 dopant. When synthesizing semiconductors, using very low concentrations of dopant can retain the electrochemical

properties of the bulk material, rather than the properties of the dopant (Sanchez et Al, 2005). The second highest peak, 14°, is the primary peak indicating the presence of molybdenum disulfide. A very narrow peak at this location lends evidence to support a larger crystal size for molybdenum disulfide and serves as an indicator that the milling and annealing phase was less effective for this component, due to its inherent anti-friction properties and resistance to fine milling (Lee et. al., 2010). Further milling would likely have had little impact on reducing particle size of MoS_2 particles. Lower peaks for TiO_2 were present at 39 °, 48 °, and 54 °, while lower peaks for molybdenum disulfide were present at 40 ° and 63 °.

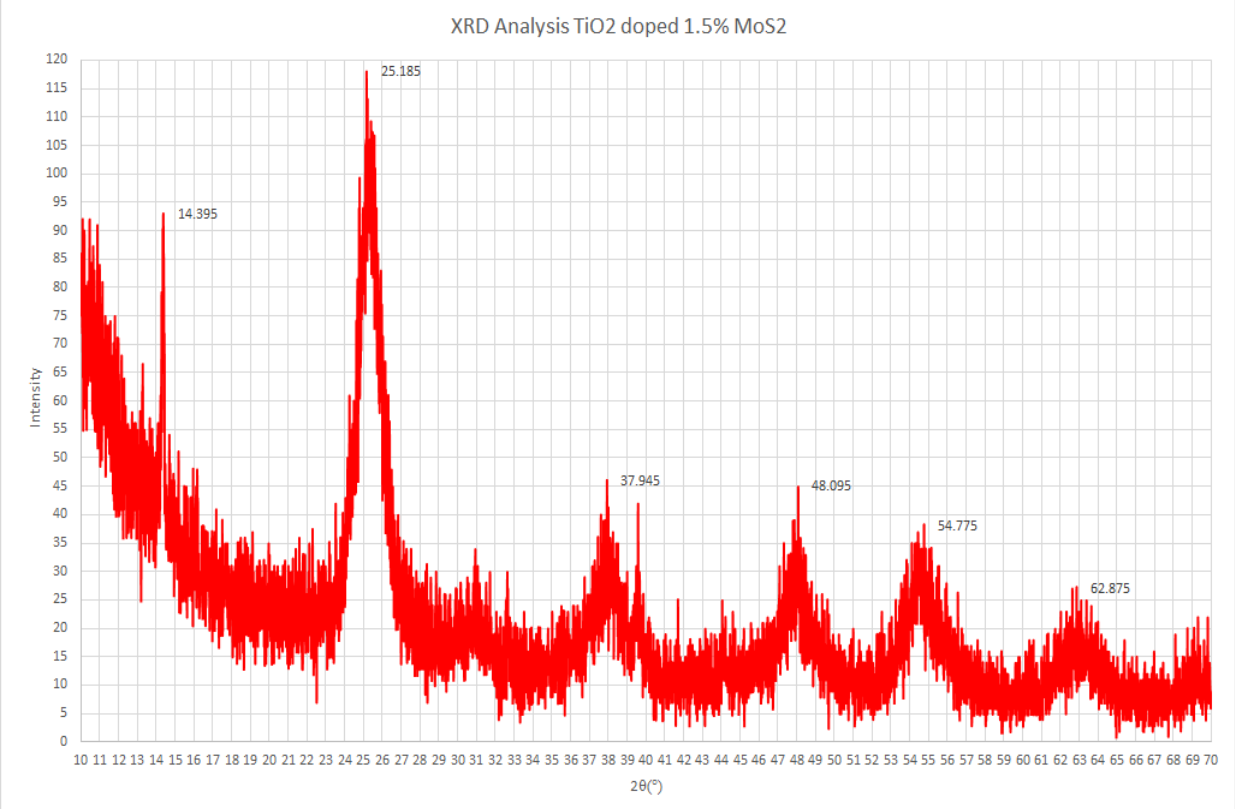

Figure 5: XRD Analysis of 1.5% MoS_2-98.5% TiO_2

The analysis of 5% MoS_2-95% TiO_2 XRD yielded promising results of a mid-level concentration synthesis (Fig. 6). Unlike the 1.5% MoS_2-98.5% TiO_2 batch where the 25° TiO_2 peak was the highest intensity, the highest intensity peak was located at 14° for MoS_2. This was a doubling from an intensity at 14° from around 95 to almost 180 between the 1.5% and 5% batches, reflecting an increase in the concentration of MoS_2 present. A switch in peak dominance from TiO_2 to MoS_2 could potentially result in decreased photocatalytic efficiency, relative to the 1.5% batch where TiO_2 is dominant (Kun et al., 2010). The third highest peak at 40° also indicates an increased concentration of MoS_2. The two key peaks for MoS_2, 14° and 40°, respectively, are of nearly identical width, indicating that milling again was not effective in decreasing its particle size. Despite this, peak width at 25° indicates success milling with respect to TiO_2, indicating that the TiO_2 had been milled into the nanometer range, and that size distribution of the TiO_2 was homogenized within the 5% MoS_2-95% TiO_2 batch. This discrepancy could result in further decreases to photocatalytic potential but is an inherent property when working with MoS_2 in the 5-10-micron range.

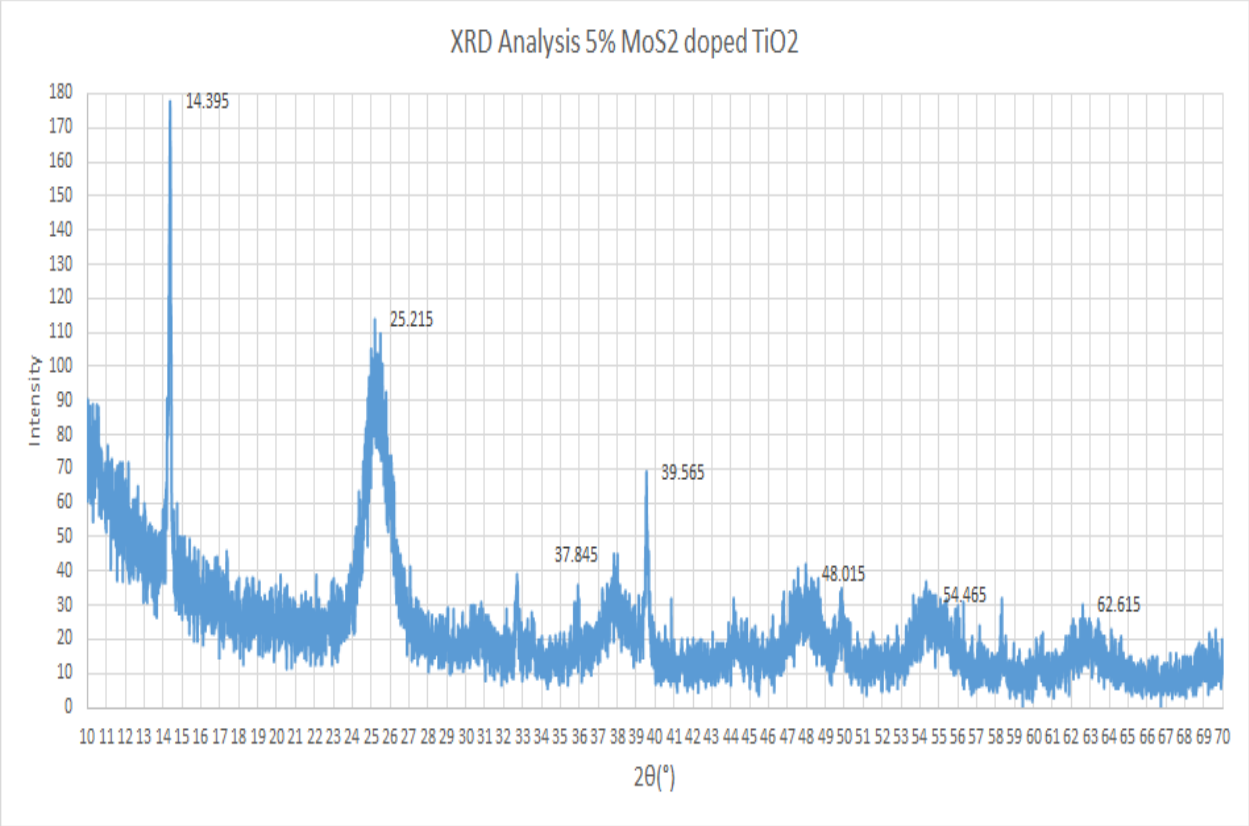

Figure 6: XRD Analysis of 5% MoS_2-95% TiO_2.

The final batch of 10% MoS_2-90% TiO_2 had the highest peak present at 14 °, demonstrating the highest concentration of MoS_2 across the samples (Fig. 7). The intensity of the 14 ° peak reached 300, roughly 40% higher than the 5% MoS_2-95% TiO_2 batch. This peak is very thin, which means again that milling of this batch was not effective in reducing the particle size of MoS_2. An increase in intensity for MoS_2 corresponds to a decreasing intensity of the 25 ° peak for TiO_2, with a decrease in intensity of around 20 at that location from the 1.5% to 10% batch. The third highest peak at 40 ° increased from an intensity of 70 in the 5% batch, to an intensity of 100 at the 10% batch, a 30% intensity increase for the MoS_2 peak. Lower intensity peaks present at 32°, 44°, 50° and 58 ° are indicative of MoS_2, while tertiary peaks at 38°, 48° and 55° are representative of the presence of TiO_2.

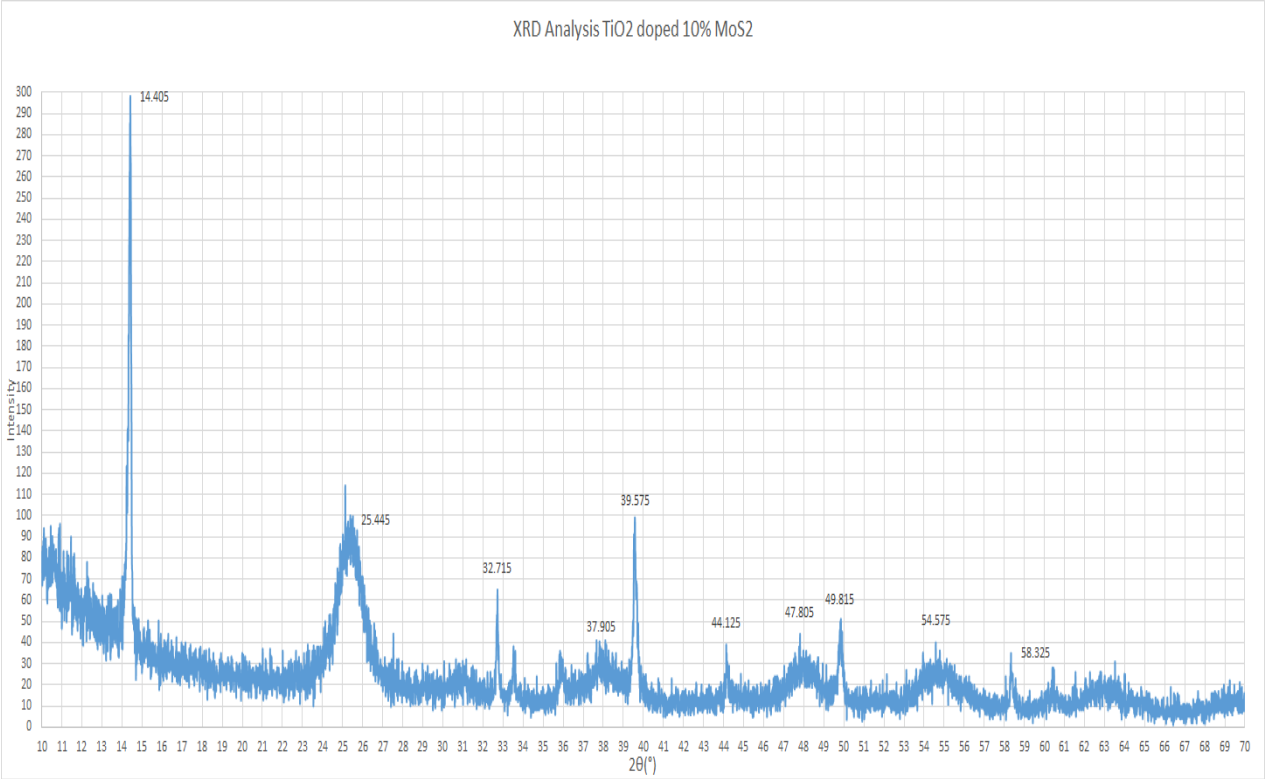

Figure 7. XRD Analysis of 10% MoS_2-90% TiO_2.

UV-Vis results:

Ultraviolet-visible spectroscopy is an analytical tool employed to analyze absorption or transmission properties of a substance through the ultraviolet (10-380 nm) and visible (380-780) wavelengths of the light spectrum. Analysis was performed at the Advanced Materials Research Facility, USF Tampa.

Titanium dioxide [TiO_2] is a vivid white colored powder employed as a paint pigment. A key property of TiO_2 is its absorption of ultraviolet light, making it an excellent ingredient in sunscreens and protective coatings (Chen and Mao, 2007). Due to ultraviolet absorptive properties, TiO_2 is an excellent photocatalyst as demonstrated by the Honda-Fujishima effect. Despite these excellent properties, pure TiO_2 has virtually no absorption in the visible wavelengths. It is theorized, based on Beer-Lambert's Law, that

integration of TiO_2 with molybdenum disulfide (MoS_2) will increase the intensity of absorption throughout the ultraviolet-visible spectra. This is due to the role of MoS_2 as an absorptive species (Forsberg et al., 2016). MoS_2 possesses a blackish-grey color, which upon doping into TiO_2 will impart the nanocomposite with the quality to absorb throughout the visible spectra. An increase in absorption will correspond relative to the increasing concentration of MoS_2, and thus will indicate successful synthesis across batches. It should be noted that an increased absorption of light is not directly correlated to increased photocatalytic activity but simply to the amount of light energy absorbed by the material at a particular wavelength.

Wavelengths from 100-280 nm are in the UV-C spectrum. This spectrum is almost completely absent in outdoor light as it is fully absorbed by the ozone layer. Wavelengths from 280-315 constitute the UV-B spectrum. The majority of the UV-B spectrum is absorbed by the ozone layer but is present in natural light at around 0.0015%. Finally, the UV-A spectrum ranges from 315-380 nm; this wavelength is not absorbed by the ozone layer or atmosphere. It constitutes around 95% of the ultraviolet light reaching the surface of the earth, or around 2.85% of total light (Matsumi and Kawasaki, 2003).

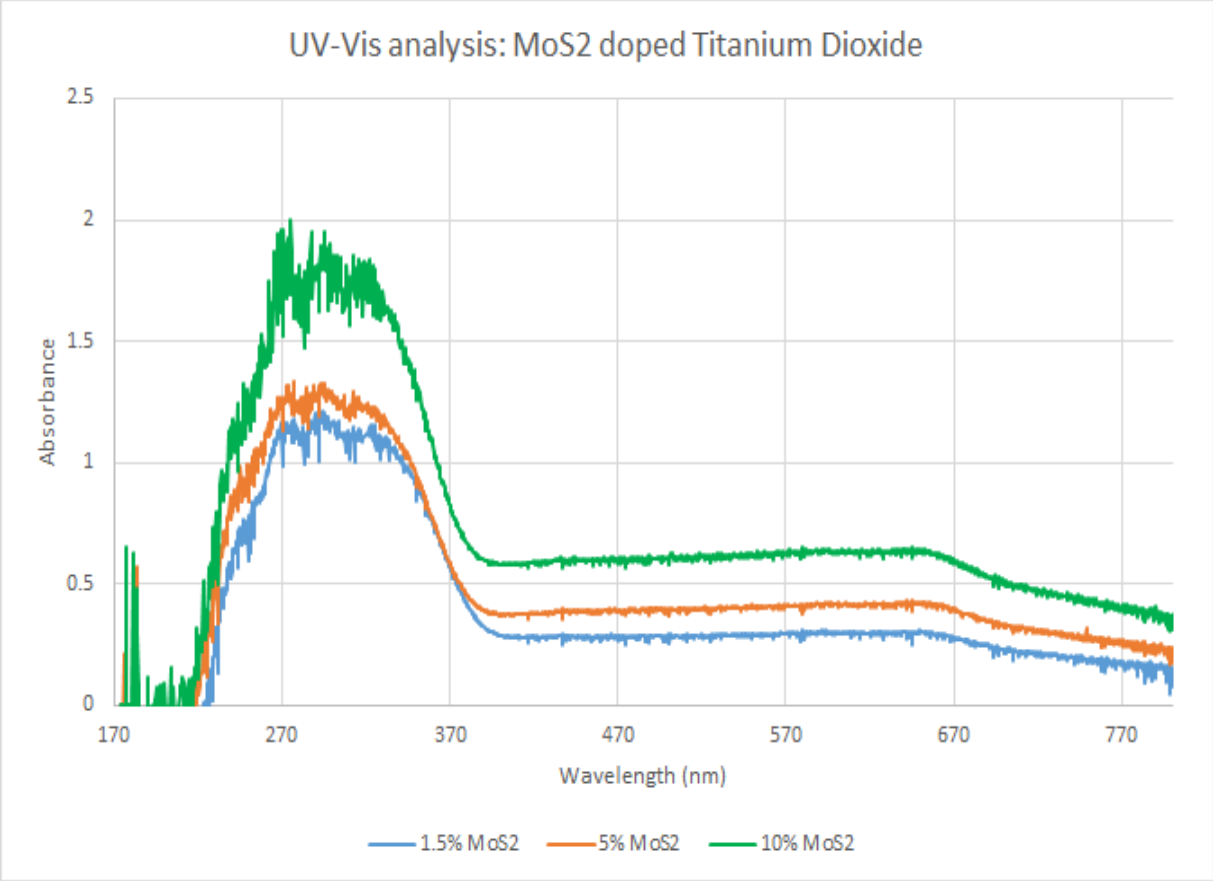

Figure 8: UV-Vis analysis overlay of the three batches MoS_2-TiO_2.

Results indicate that the sample containing the highest concentration of MoS_2 (10%) had the highest intensity of absorbance throughout the spectra (Fig. 8). In particular, this sample absorbed far more light between 250-350 nm than the other samples, roughly 50-60% more than 5% MoS_2- 95%TiO_2 in the same wavelengths. Despite this, all samples absorbed elevated amounts of light between 220-380 nm. This is due to the high concentrations of TiO_2 in each of the samples. This is a clear indicator of successful synthesis through Beer Lambert's Law, as even gaps in absorbance between the MoS_2-TiO_2 batches can be seen.

Key areas to note in the readout are between 220-230 nm, as well as 350-380 nm. Between 220-230 nm, the smallest differences in absorbance are observed between 1.5% MoS_2-98.5% TiO_2 and 10% MoS_2-90% TiO_2. This demonstrates that doping has little

effect on the intensity of absorbance within the given wavelength. One of the most interesting areas is between 350-380 nm, where 1.5% MoS_2-98.5% TiO_2 and 5% MoS_2-95% TiO_2 batches, but not 10% MoS_2-90% TiO_2 batch, share the same levels of absorbance despite differences in concentration. This could be due to an overlap in that wavelength where absorbance is independent of concentration between 1.5% and 5% MoS_2. MoS_2 acts as an effective absorbent of light for all of the samples within the visible spectrum; even the lowest concentration, 1.5% MoS_2, had measurable levels of absorption throughout the visible spectra, illustrating its role as an effective tool for extending the absorbance of TiO_2 into the visible spectra. Successful synthesis is again demonstrated by readings in the visible spectra, with 10% MoS_2 absorbing the most light and 1.5% MoS_2 absorbing the least.

Fourier-transform infrared spectroscopy (FTIR) results:

FTIR is an analytical tool used on solid or liquid samples to identify functional groups present in a substance. FTIR reveals the vibration bonding structure of a chemical, and is dependent upon which functional groups and elements it possesses. Vibrational bonding is displayed as the absorption of light at a particular area of the spectrum where a chemical is being excited, and is identifiable by an FTIR machine. FTIR analysis was employed in this experiment to analyze the changes in structure of the TiO_2 nanocomposite when it is doped with 1.5%, 5% and 10% concentrations of MoS_2. This was accomplished by running samples of pure TiO_2 and MoS_2 and comparing the synthesized batches to these standards. Changes in these FTIR readings indicate whether changes in crystal structure are occurring when the concentration of MoS_2 is increased.

FTIR spectra consist of X and Y axes, the X axis demarcating wavenumber and the Y axis expressed as a percentage of the absorption or transmission of light. Transmission is the ratio between the intensity of light passing through an analyte (I) and the intensity of the incident light source (I_o):

$$T = I / I_o$$

$$\%T = T * 100$$

The value of transmittance readings is that they illustrate the fraction of photons from a monochromatic beam of light which passes through a sample and is not absorbed. If a chemical has a transmittance value of 0.6, 40% of the photons are being captured by the chemical, and the other 60% of photons pass through. Transmittance is given on a scale from 0 to 0.99.

Absorbance is a measurement of the potential of a chemical to absorb light which hits its surface, given as the equation:

$$A = \log (I/I_o)$$

Where I equals the intensity of light passing through an analyte, and I_o equals the intensity of the incident light source.

Transmission and absorption are logarithmically inverse to each other, demonstrated by the equation:

$$A = \log_{10} (1/T)$$

Where A is absorbance, and T is the transmittance. For this analysis, transmittance was used for the readouts.

Analysis was performed at the University of South Florida St. Petersburg on a Shimadzu Iraffinity-1S system coupled with a Quest ATR Diamond GS10800-X solid

sample analysis accessory. Standards of TiO_2 and MoS_2 were obtained by Sigma Aldrich, with the MoS_2 standard being the same stock used during synthesis of the complex. Analysis was performed across the mid-infrared range from 400-4000 cm^{-1}. Samples were individually analyzed and then overlain to create a composite readout (Fig. 9).

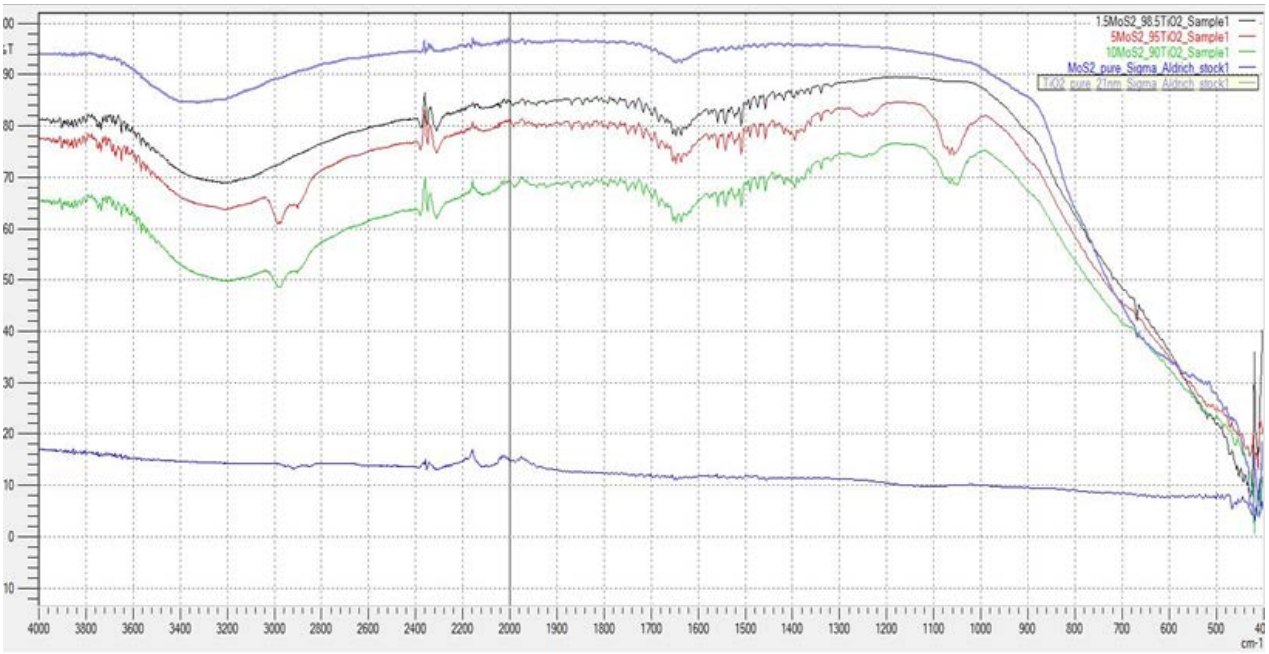

Figure 9: FTIR analysis overlay of synthesized batches and chemical standards

The compound with the highest transmittance through the mid infrared was the TiO_2 chemical standard. This is one of the inherent properties of TiO_2 that allows it to be an integral component in paints by preventing heat absorption and acting as a white pigment. The compound with the lowest transmittance in the reading was the MoS_2 standard. This is also to be expected and is one of the key reasons MoS_2 was employed in the experiment for its known role as an absorptive species. Key indicators for the TiO_2 standard are noted from 3700-2500 cm^{-1} as well as from 1700-1600 cm^{-1}. At around 1000 cm^{-1}, TiO_2 sharply decreases in transmittance. This decrease starts from around 10% of photons transmitted at 1000 to 80% of light transmitted at 400 cm^{-1}. These characteristics can be used to identify the presence of TiO_2 in the synthesized batches of nanocomposite. Key transmission peaks present in the MoS_2 spectrum are present at 2400-2320 cm^{-1}, 2200-2120 cm^{-1}, 2080-1980 cm^{-1}, and 1980-1940 cm^{-1}, with two small troughs from 2960-2840 cm^{-1}. These measurements can be used to analyze for the presence of MoS_2 in the synthesized batches.

The spectra for the synthesized batches reveal first that from 4000-800 cm^{-1} an increasing concentration of MoS_2 linearly corresponds to increases in absorption. For example, at 3200 cm^{-1} pure titanium dioxide had an absorbance value of 0.0655, 1.5% MoS_2- 95% TiO_2 had an absorbance value of 0.1612, 5% MoS_2-95% TiO_2 had a value of 0.1938, and 10% MoS_2-90% TiO_2 had a value of 0.301. From 4000-800 cm^{-1}, none of the readings overlap and are stacked relative to the concentration of MoS_2, with pure TiO_2 exhibiting the lowest absorption and 10% MoS_2-90% TiO_2 displaying the highest absorption. In addition, all three batches displayed the characteristics of pure TiO_2, with transmittance decreases located at both 3700-2500 cm^{-1} and 1700-1600 cm^{-1}. Also, they

all displayed sharp decreases in transmittance from 1000-400 cm^{-1}. All of the batches displayed transmittance peaks from 2360-2280 cm^{-1}, 2200-2120 cm^{-1}, and 2040-1980 cm^{-1}. This resulted from constructive interference between peaks located at the same locations on both pure TiO_2 and pure MoS_2.

Key discrepancies to note in the spectra are the presence of three transmission troughs located 3040-2800 cm^{-1}, 1280-1200 cm^{-1}, and again at 1120-980 cm^{-1} for the 5% and 10% MoS_2 batches, but not the 1.5% MoS_2 batch. The troughs at 3040-2800 cm^{-1} can be explained by the presence of a similar anomaly from 2960-2840 nm in the pure MoS_2 sample. Despite this, there is little explanation offered in the graph for the troughs at 1280-1200 cm^{-1} and 1120-980 cm^{-1}, as both TiO_2 and MoS_2 standards are nearly flat-lined at these locations.

SEM results:

Scanning Electron Microscopy (SEM) is an analytical tool with practical applications in materials chemistry. It can be used to show the surface structure and shape of a synthesized material, as well as particle size. Analysis was performed at the USF Tampa Nanotechnology Research Education Center on a Hitachi model SU 70 scanning electron microscope. The goal of this analysis was to evaluate particle size of the MoS_2-TiO_2 molecules post-milling, as well as to ascertain the structures and bonding generated between the two materials. Key indicators of successful synthesis demonstrated by the SEM images are particle sizes between 5-20 microns to optimize photocatalytic activity, as well as uniform distribution of the nanoparticles.

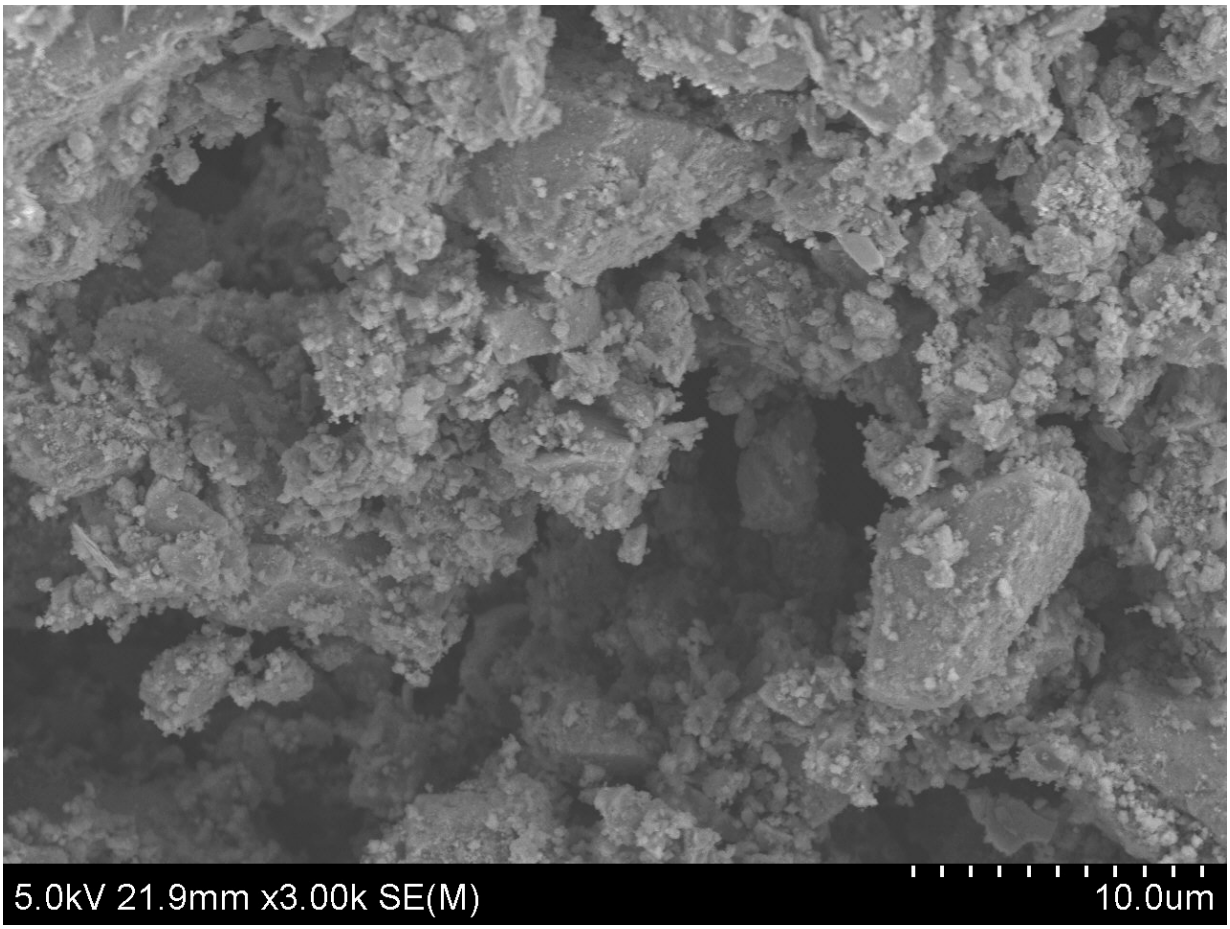

Figure 10: 1.5% MoS_2-98.5% TiO_2 SEM readout

Analysis of the 1.5% MoS_2-98.5% TiO_2 batch provided valuable information as to its microcrystalline structure as well as particle size. MoS_2 flakes (large linear structures) can be seen coated in small white nodules (TiO_2) in Fig. 10. The particle size of TiO_2 bonding onto the MoS_2 flakes is quite small, in the 1-micron range. This compares to the MoS_2 flakes in the 5-10-micron range. This size difference could be attributed to the anti-friction properties of MoS_2 (Chen and Mao, 2007); thus, milling may have had less of an effect on the MoS_2 structures. Despite size differences, bonding can clearly be seen as an abundance of TiO_2 particles coat the MoS_2 flakes. This compares to SEM images of TiO_2 synthesized through the Sol-Gel method (Chenari et al., 2016). These nanoparticles

exhibit similar shape and texture to that of those generated in the 1.5% TiO_2 batch, indicating successful milling and synthesis (Fig. 11).

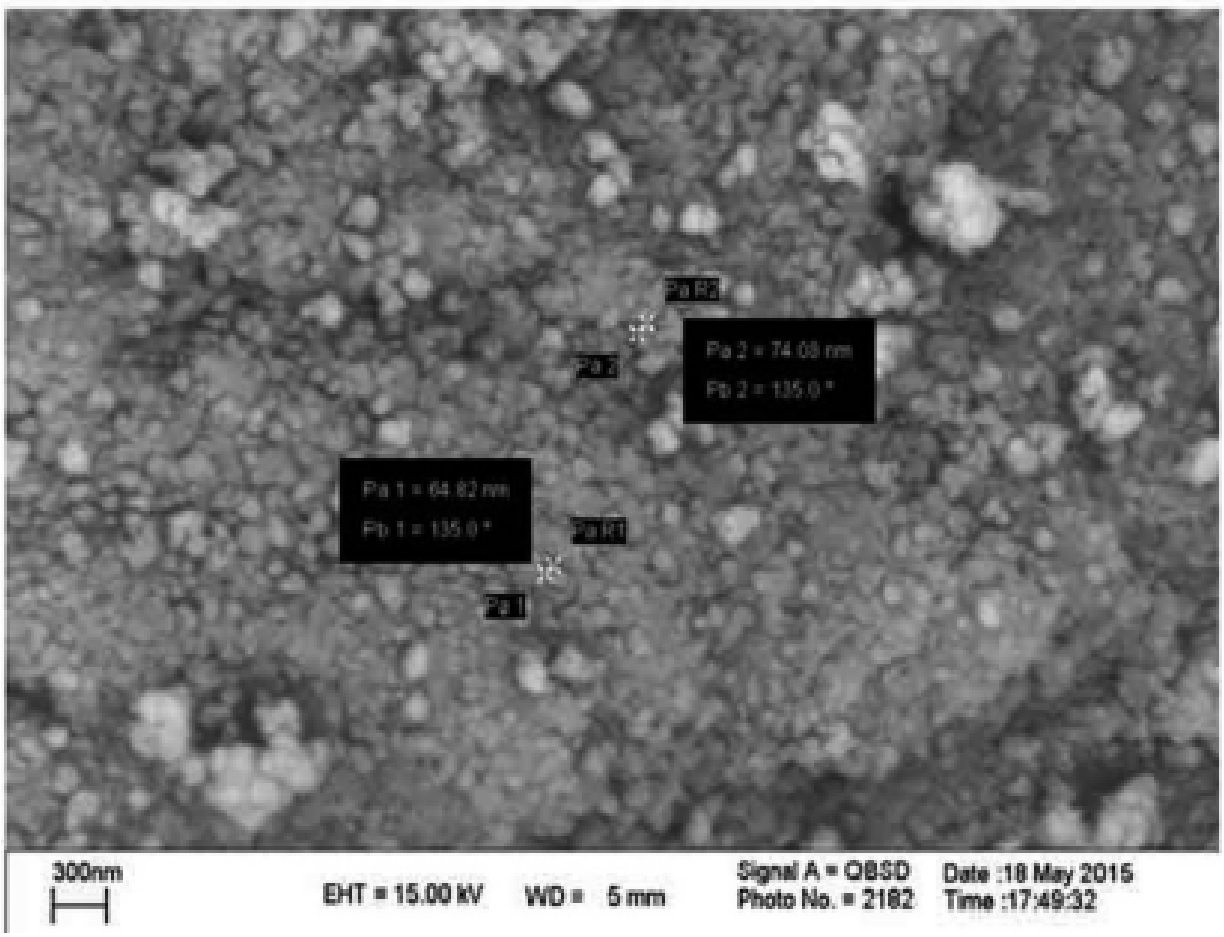

Figure 11: TiO_2 nanoparticles as seen under SEM (Chenari et al., 2016).

In the 5% MoS_2-95% TiO_2 sample, adhesion can once again be seen between fine TiO_2 clusters, and larger MoS_2 flakes (Fig. 12). The SEM image contains a wider range of MoS_2 flake sizes, relative to the imaging from the 1.5% MoS_2-98.5% TiO_2 batch (Fig. 10). In the left side of the image, 4-5 micron MoS_2 flakes can be seen coated in a fine TiO_2 layer. This surface bonding of TiO_2 particles thus occurs on large and small sized MoS_2 flakes and across the MoS_2 concentrations. This can be expected from the sol gel process, as the reduction of titanium isopropoxide to TiO_2 results in precipitation and

formation of bonds between the two substances. A key indicator of successful synthesis in this batch is the absence of layering between the MoS_2 flakes, as evidenced by visual similarity to SEM photographed MoS_2 single layer Nano sheets in Fig. 13. This is due to the use of surfactant, isopropanol as a solvent, and extensive sonication of the MoS_2 suspension before the introduction of titanium isopropoxide. The combination of these methods was responsible for breaking the Van-der-Waals bonds typically present between layers in MoS_2 (Forsberg et Al., 2016).

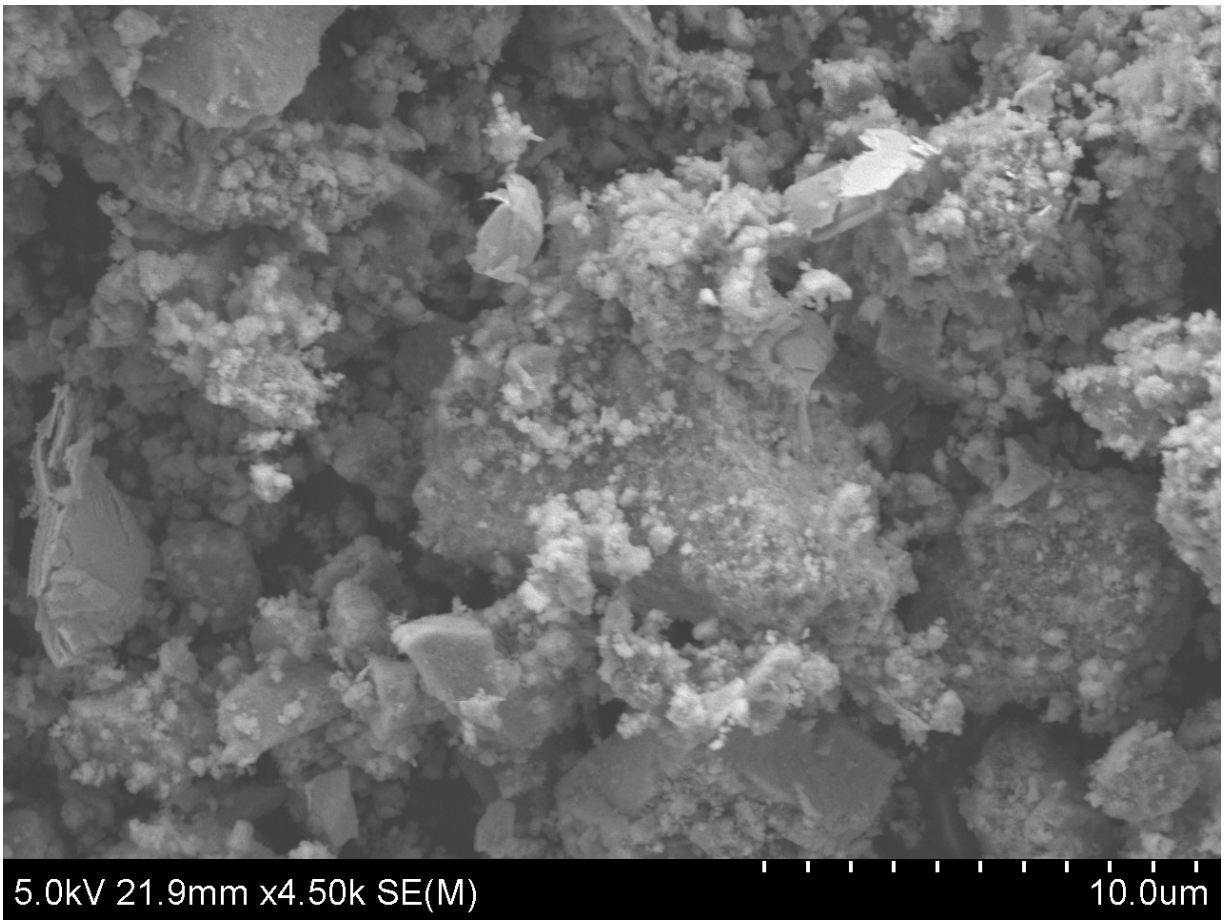

Figure 12: 5% MoS_2-95% TiO_2 SEM readout

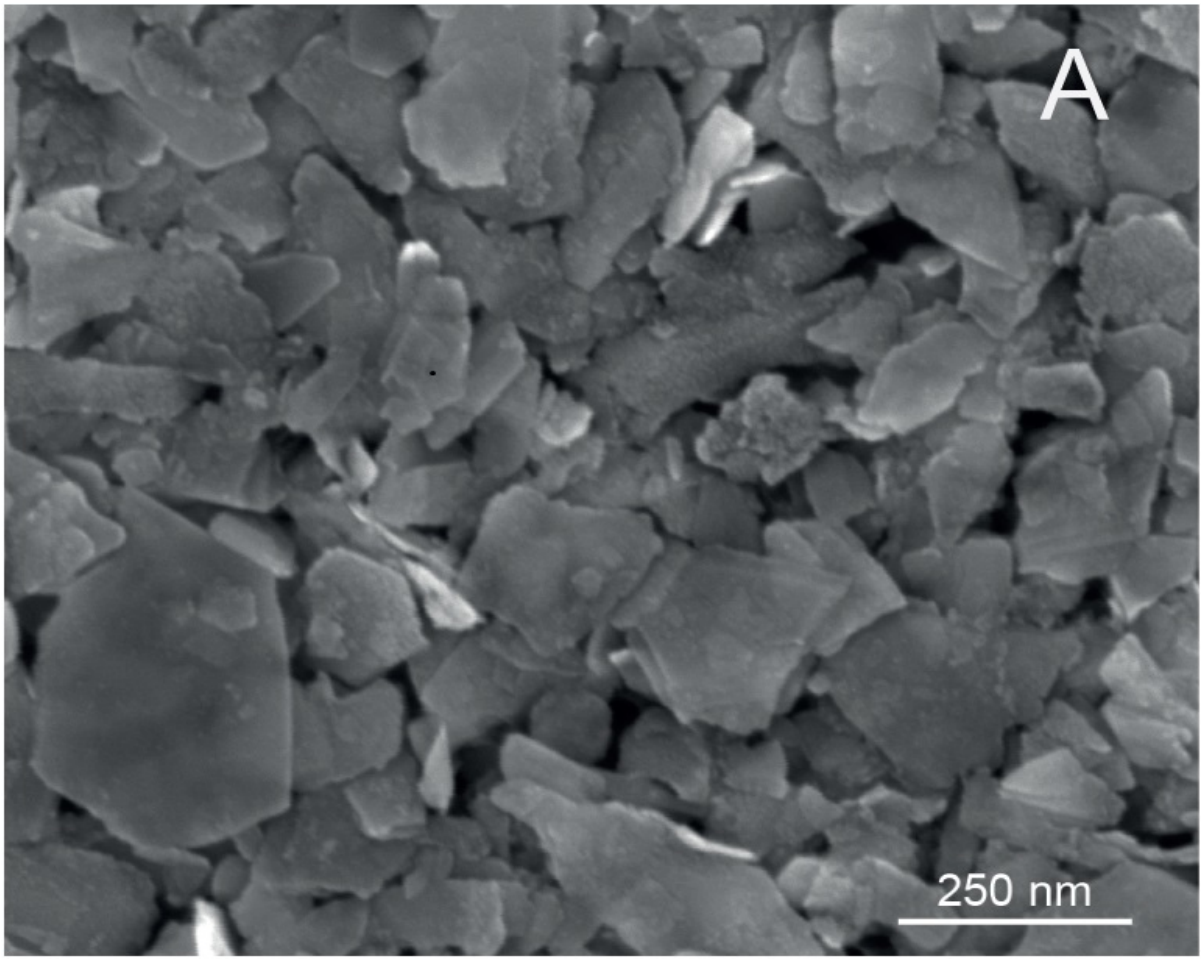

Figure 13: Bulk mono-layered MoS_2 flakes under SEM (Forsberg et al., 2016).

In Figure 14, a full coating of a hexagonal layered MoS_2 structure in TiO_2 particles can be seen in the 5% MoS_2-95% TiO_2 sample batch. A surface bonding of TiO_2 to MoS_2 can again be inferred from the SEM image. The largest MoS_2 particle picture spans around 4 microns, with TiO_2 molecules again distributed in the 1-micron size range.

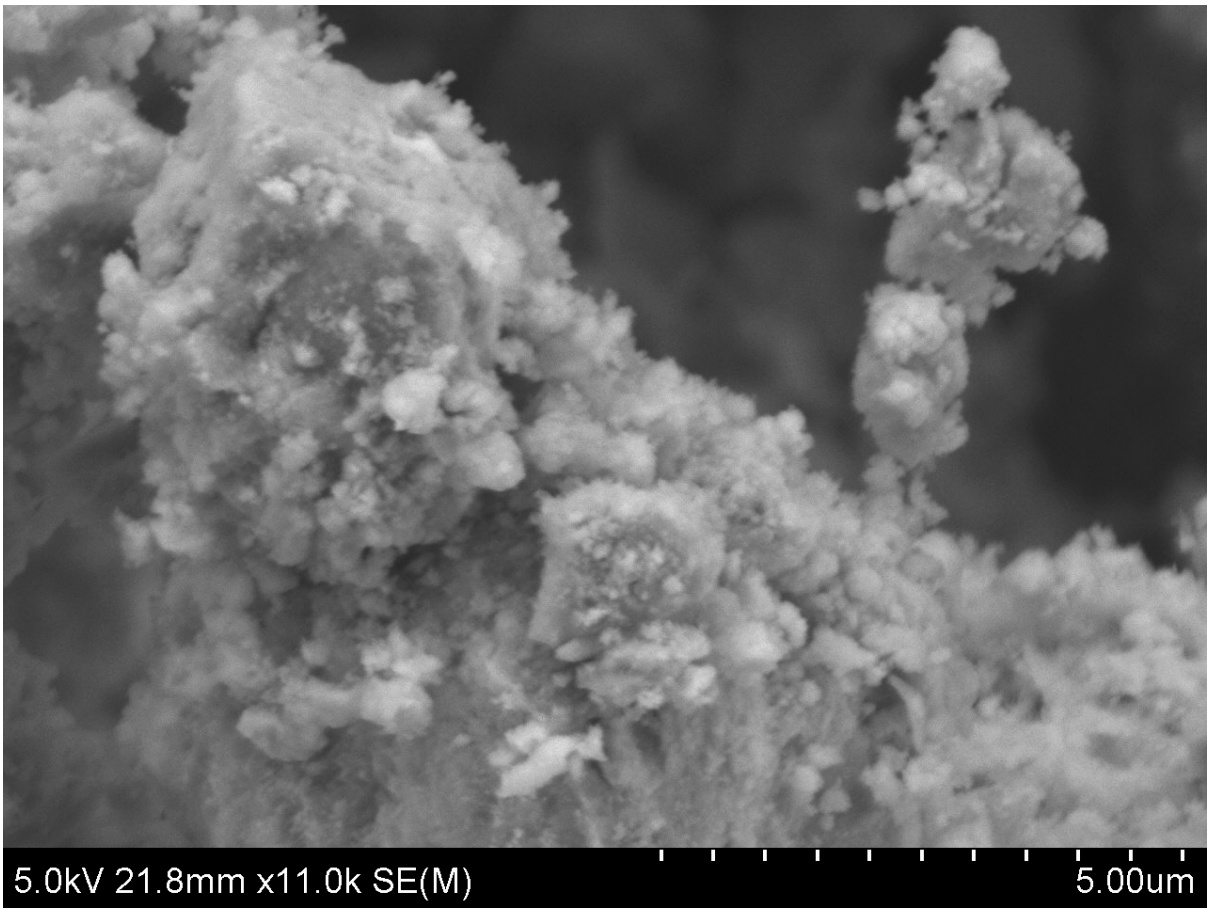

Figure 14: 5% MoS_2-95% TiO_2 readout #2

The final sample batch analyzed was that of 10% MoS_2-90% TiO_2 blend (Fig. 15). This batch had surface characteristics similar but not identical to the 1.5% and 5% MoS_2 concentration batches. These images contain the largest MoS_2 flakes, possibly due to increased anti-friction properties of the MoS_2. This property could result in the prevention of effective milling at higher concentrations, thus yielding larger particle size post-milling. Nevertheless, bonding can still be seen between the MoS_2 flakes and the TiO_2 nodules. In the left side of the image, a fully coated MoS_2 flake can be seen next to a second MoS_2 flake with a light coating of TiO_2 across the surface structure.

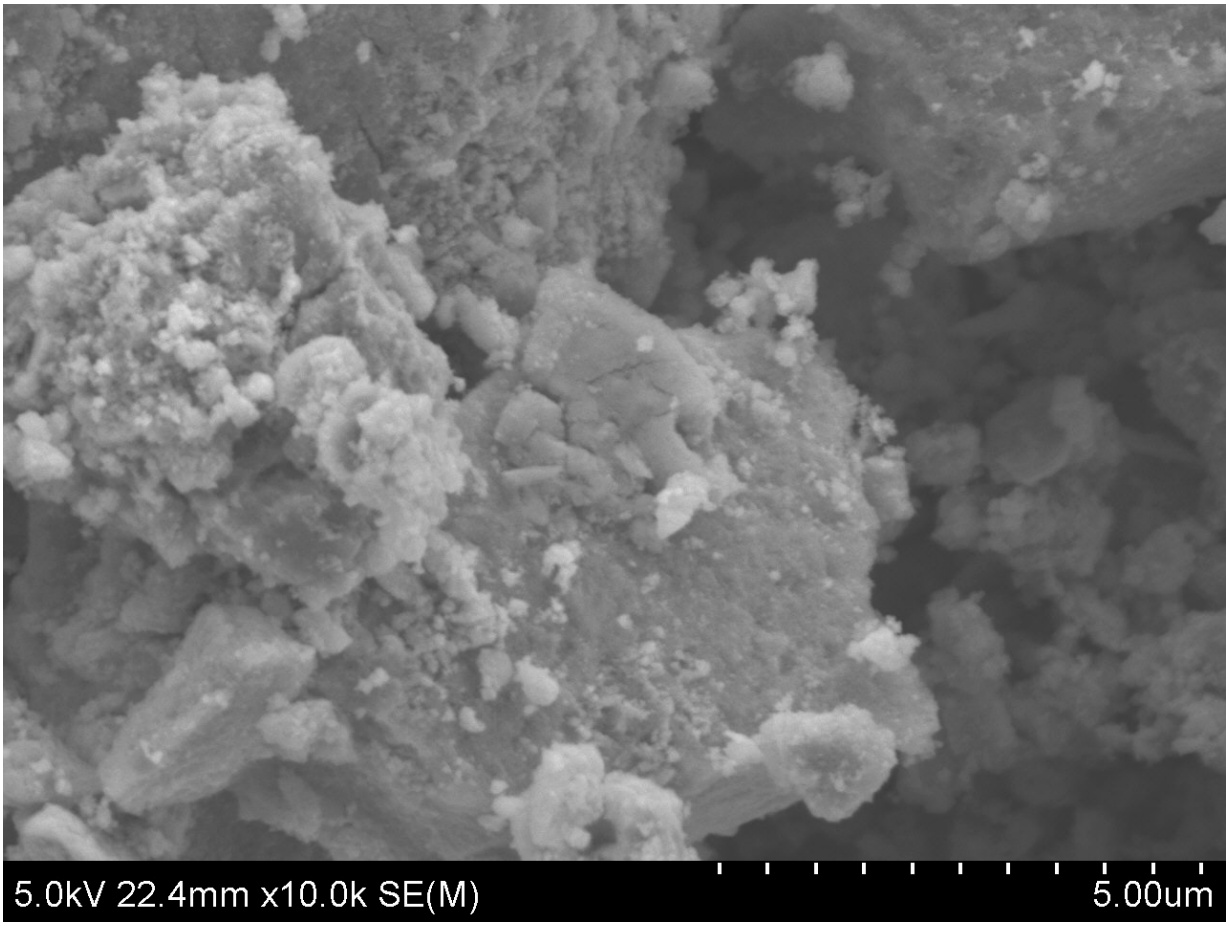

Figure 15: 10% MoS_2-90% TiO_2 SEM readout

The last SEM reading depicts a large MoS_2 flake coated in TiO_2 nanoparticles in the 10% MoS_2-90% TiO_2 batch (Fig. 16). Particle size readouts are given.

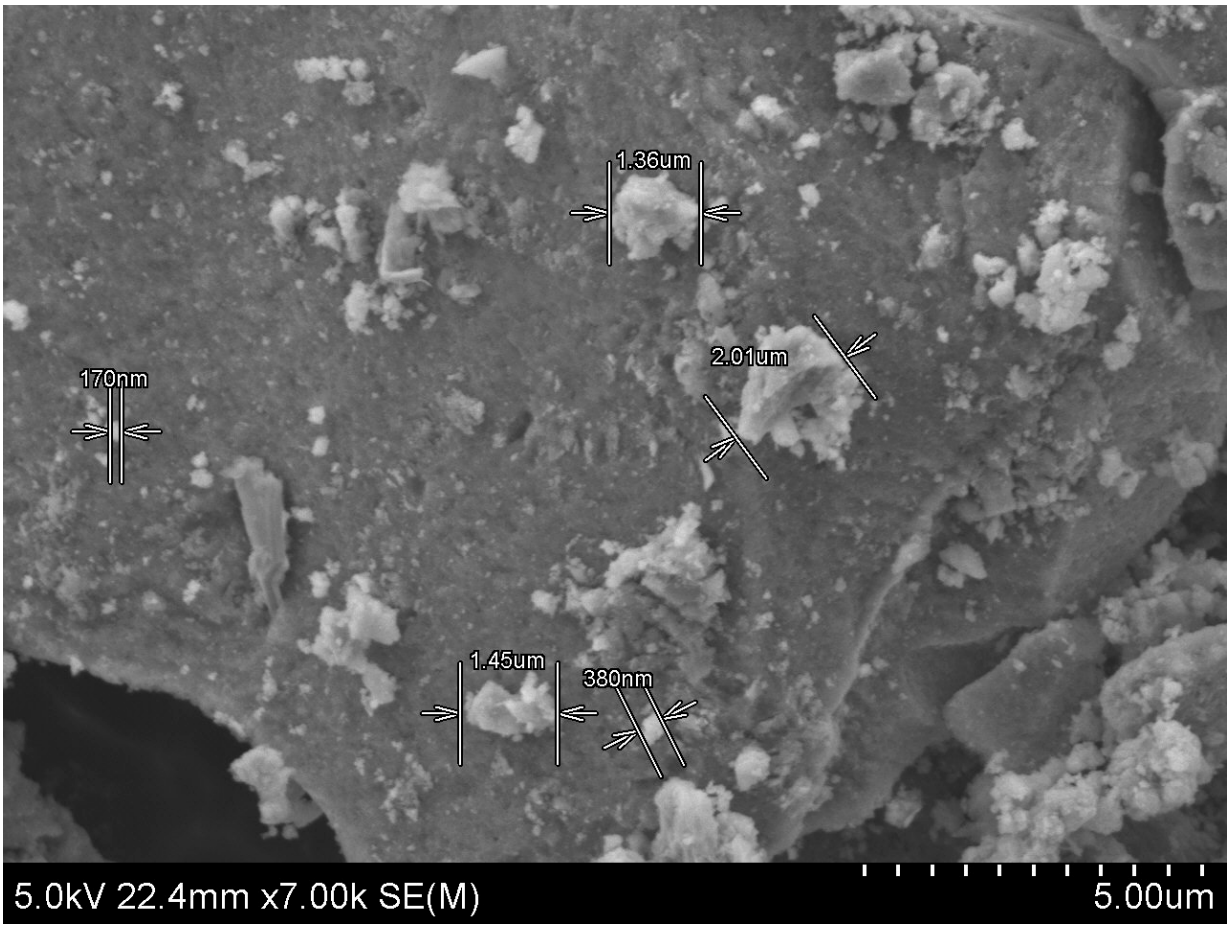

Figure 16: 10% MoS_2-90% TiO_2 SEM readout #2.

Chapter 3: Testing the Effectiveness of MoS_2-TiO_2 in Water Disinfection

Background

After completion of the synthesis and characterization phases, the final objective was to integrate the nanomaterial into a useful platform for generating potable water and to test its efficiency in disinfecting water. Testing was employed to determine if disinfection time was indeed decreased through the doping of titanium dioxide with varying concentrations of molybdenum disulfide. A reduction in disinfection time could prove beneficial in an emergency scenario where large quantities of potable water are required, as a shorter disinfection time would result in greater turnover of disinfected water within the same timeframe. All three synthesized varieties of nanomaterial (1.5% MoS_2– 98.5% TiO_2, 5% MoS_2– 95% TiO_2, and 10% MoS_2 – 90% TiO_2) were tested in the solar disinfection platform. These results were then compared to disinfection rates without the use of nanomaterial, and disinfection utilizing pure TiO_2 obtained from Sigma- Aldrich.

Experimental setup

A key goal of this project was to utilize a simple design which could easily be replicated and deployed quickly in an emergency scenario. This involves utilization of a design with readily available, cheap materials. The chosen design was the solar disinfection platform, which is accepted by the World Health Organization as a primary disinfection strategy for waterborne bacteria. Acetate sheets (projection transparencies)

were utilized in conjunction with silicone adhesive to produce the nanomaterial inserts. One-liter bottles composed of polyethylene terephthalate were employed for the experiments to standardize volume and to provide an amount of water which could more realistically meet hydration requirements, versus a smaller sample size. A key benefit in the simplicity of this design is that large quantities of inserts can be shipped to emergency areas cheaply and employed immediately for generating potable water within standard water bottles. Light intensities during experimentation were kept below the maximum intensity of sunlight hitting the earth with attenuation (1,080 W/m^2) utilizing a full spectrum bulb.

Evaluation of efficacy was performed utilizing a standardized level of Escherichia coli [E. coli], which is a commonly used indicator of fecal contamination in water (Odonkor and Ampofo, 2013). Deionized water was purposefully inoculated with E. coli bacterial culture to serve as a "contaminated" water analogue with between 300 and 3000 colony-forming units per milliliter [CFU/ml]. The water samples were then exposed to light emanating from a Chromalux 100 W full spectrum bulb, calibrated to an intensity comparable to that of direct overhead sunlight. This was ensured through the implementation of a SP-215 Apogee Precision Amplified Pyranometer coupled with Vernier light intensity monitoring software (Fig. 17). Quantitative data collection was employed through plating and culturing of 100 µL samples of water onto agar media in 30-minute intervals throughout the disinfection experiments. Use of a nanomaterial insert that results in a total disinfection of the water within a shorter time-period than the others could be considered objectively superior to other nanomaterial blends.

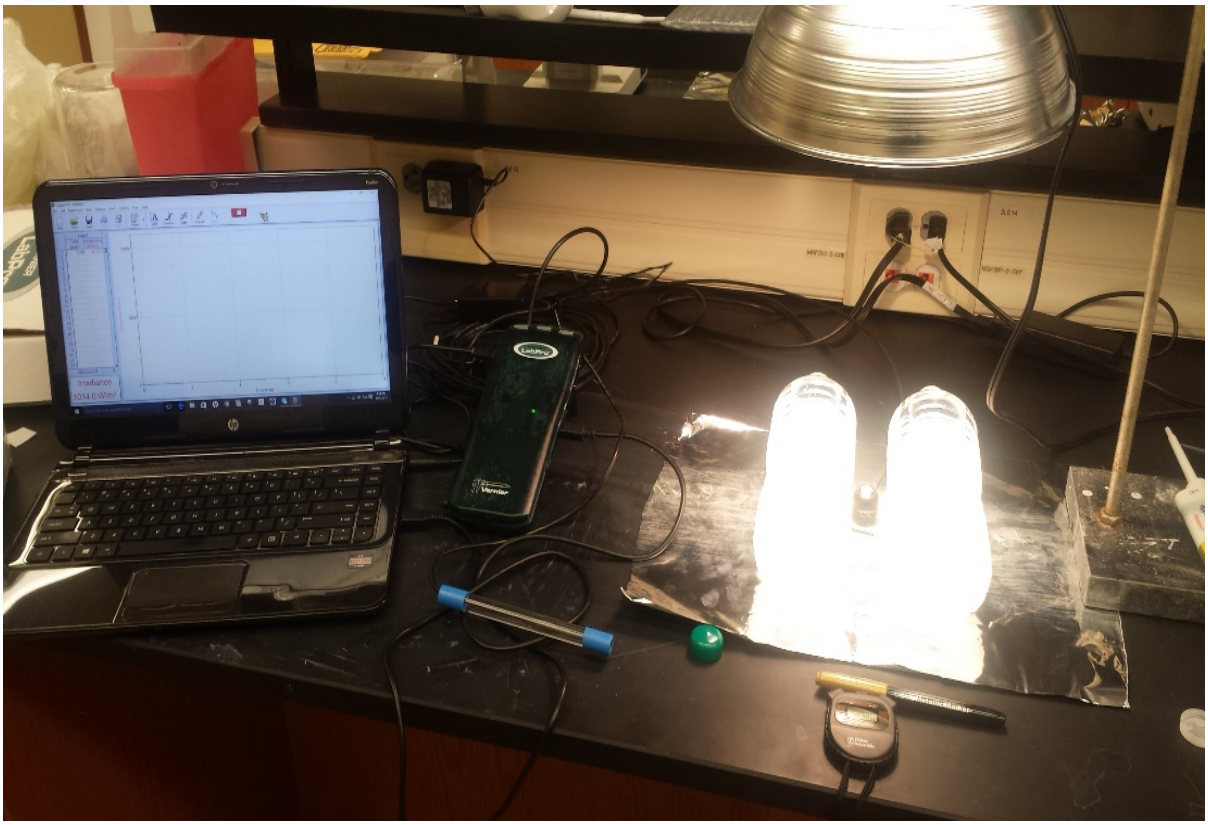

Figure 17: Experimental solar disinfection setup with bottles and pyranometer

Preparation of nanomaterial inserts

Immobilization of pure TiO_2 and MoS_2-TiO_2 powders was accomplished by applying a coat of clear silicone sealant across the clear acetate sheets using bristle brushes. Clear silicone, rather than colored silicone was employed as a bonding agent. This eliminates the addition of additional pigments within the silicone which have the potential to act as an absorptive species, skewing experimental results intended to elucidate the effectiveness of the different nanomaterial blends. In particular, black silicone contains charcoal which would potentially skews results. Only one type of powder was applied to each sheet, rather than a mixture of powders. Pure TiO_2 sheets were prepared first, followed by 1.5% MoS_2-TiO_2, then 5% MoS_2-TiO_2, and finally 10% MoS_2-TiO_2. The workspace was cleaned thoroughly between the preparations of batches,

to prevent cross contamination. These powders were evenly spread across the surface using a sieve, fully coating the silicone. Excess powder was shaken off, and then allowed to cure for 24 hours in complete darkness. This process yielded water resistant inserts of nanomaterial embedded onto silicone, which could be exposed to water without the powder coating washing off.

These coated inserts were then cut down to size (8.5 x 5 inches) and stored in aluminum foil to prevent potential oxidation or photo degradation. When ready for use, these sheets were rolled up and placed into the 1-liter non-UV resistant polyethylene (PET) bottles, coating side facing upwards (Lonnen et al., 2005).

Preparation of E. coli broth suspension

A Lysogeny broth [LB] stock solution was prepared by adding 25 grams of LB powder to 1 liter of deionized water within an autoclave-safe glass bottle. The mixture was autoclaved for 20 minutes at 15 PSI to disinfect the solution. Once the broth cooled to room temperature, it could safely be stored under refrigeration.

Preparation of agar plates with medium

A stock solution of agar broth suitable for plating was prepared by mixing 25 grams of LB broth powder and 15 grams of granulated agar in 1 liter of water in a 2-liter flask containing a stir bar. With stirring, the mixture was brought to a boil and then removed from heat. The flask containing the mixture was then sterilized in an autoclave for 20 minutes at 15 PSI. The flask was removed and the solution allowed to cool to 50 ℃, then transferred to sterile petri dishes in 20 mL aliquots. The dishes were then covered

and placed in a laminar flow fume hood, where they were allowed to set for 24 hours. After this period, the agar plates were placed in zip-lock bags and refrigerated until use.

Culturing of E. coli

Firstly, K12 strain E. coli cultured on agar was obtained from Carolina Biological Supply Co. A suspension was prepared by transferring 50 µL of the bacterial culture into 10 mL of LB broth within eight brown glass 30 mL culture vials. The silicone injection ports of the culture tubes were removed and replaced with sterile medical cotton wrap secured by screw cap to allow for the flow of air. The cultures were then allowed to colonize for 24 hours at 37 ℃ within an incubation chamber secured atop an orbital shaker for constant mixing (Fig. 18). After incubation, the culture vials were wrapped in aluminum foil and refrigerated to prevent contamination of the cultures.

Figure 18: E. coli culture vials undergoing incubation and mixing.

Immediately prior to use in experimentation, the E. coli bacterial culture was separated from the LB broth. This was achieved by transferring one of the liquid culture vials to a centrifuge tube. The mixture was centrifuged for 5 minutes at 1500 rpm, yielding a bacterial pellet from which the broth could be discarded (Fig. 20). The broth was then replaced by 10 mL of 0.85% Saline solution and agitated thoroughly by a vortex mixer to break up and suspend the bacterial pellet. One-mL aliquots of this solution were utilized per bottle during the experimentation phase.

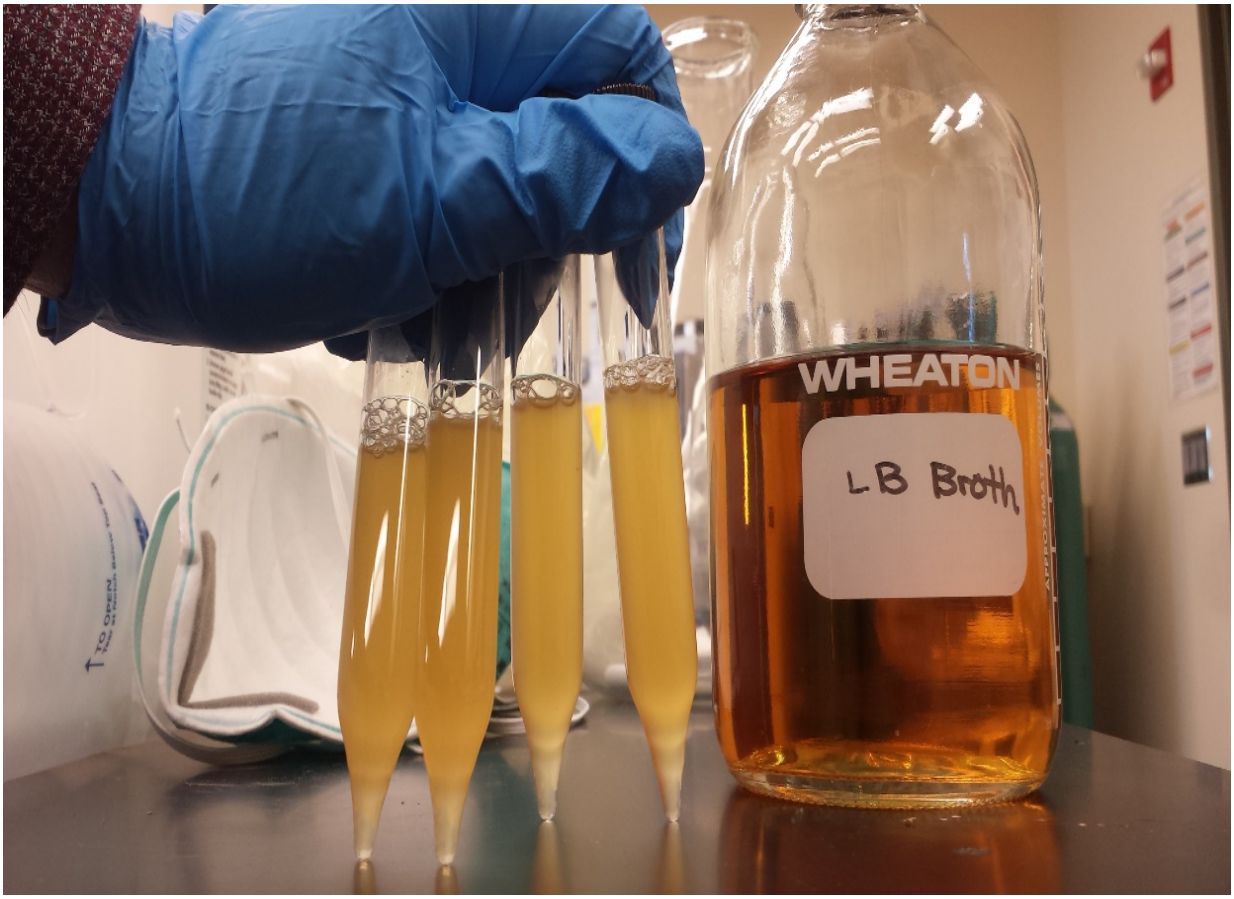

Figure 19: E. coli cultures in LB broth post incubation, compared to sterile broth

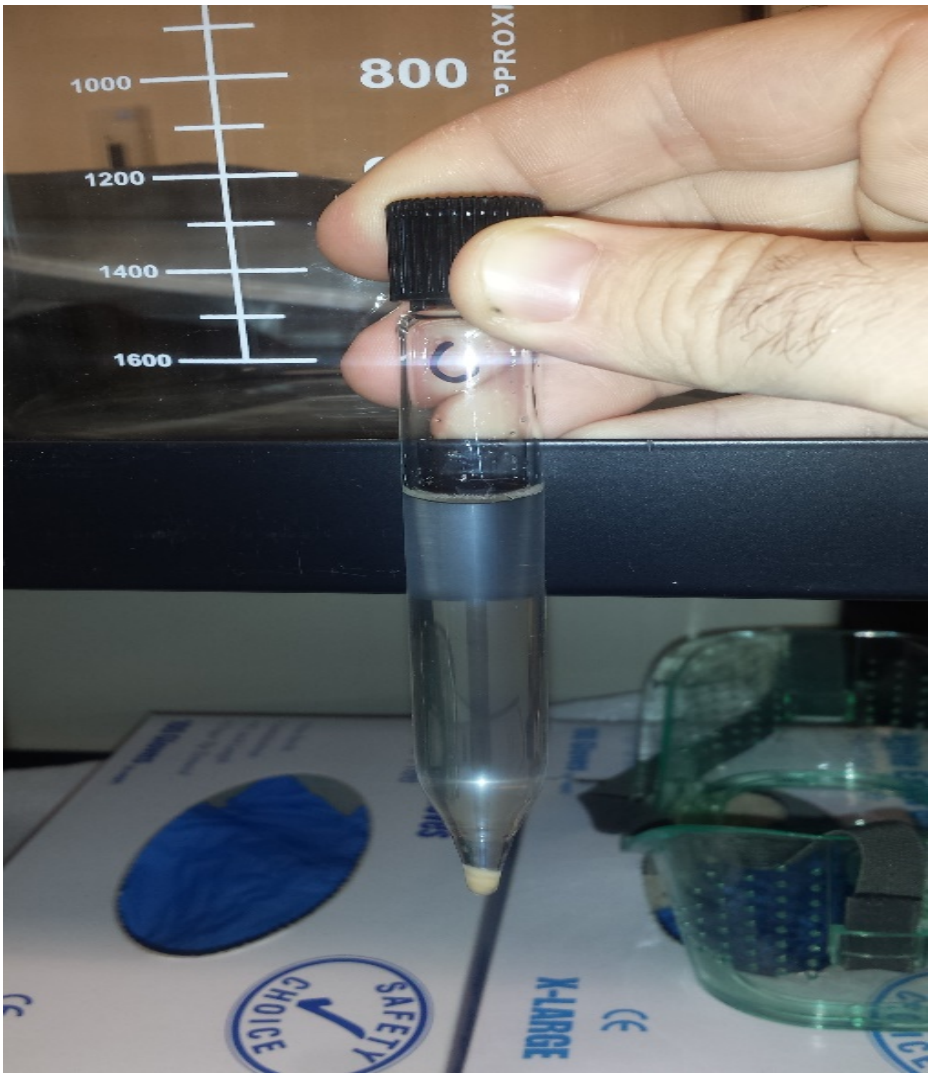

Figure 20: E. coli bacterial pellet immediately prior to resuspension

Colony count through serial dilution

100 µL of the resuspended E. coli solution in saline was added to a second centrifuge tube containing 9.9 mL of 0.89% saline solution and agitated for homogeneity. This was again diluted by removing 1 ml of solution from the second tube and transferring it to a third centrifuge tube containing 9 mL of 0.89% saline solution. The second and third test centrifuge had 100x and 1000x dilutions, respectively. This dilution was performed to achieve a target concentration of 300 to 3000 colony forming units per

milliliter. 100 µL of solution from the second and third centrifuge tubes were plated in duplicate onto agar and counted. While the 100x dilution was too numerous to count, the 1000x dilution yielded a viable count at an average of 97 colonies per plate, or 970 colony CFU/ml at a 1000x dilution. Thus, it can be expected that taking 1 mL of saline culture and diluting with 999 mL of deionized water would yield an initial count of bacteria between 30 and 300, if 100 µL samples were taken and plated prior to disinfection. Thus, a 1000x dilution factor was employed for testing when taken from the stock cultures of E. coli.

Experimental procedure: testing disinfection properties of the nanomaterials

First, a saline culture of E. coli was prepared according to aforementioned procedure and set aside. Next, acetate inserts coated with the appropriate nanomaterial were rolled up and placed into two 1-liter polyethylene terephthalate (PET) bottles. Table 2 provides details of which nanomaterial was utilized during each experiment. The bottles were then filled to the 1-liter mark with deionized water. From there, two 1 ml aliquots of E. coli saline culture were drawn up using an autopipette and injected into each of the water bottles. The bottles were agitated to distribute the bacteria. An initial bacterial count was taken by drawing up a 100 µl aliquot of water using an autopipette and depositing it dropwise onto an agar plate. The droplets were then distributed on the agar using a sterilized inoculating loop. Next, the bottles were placed, insert side up, underneath a full spectrum UVA/UVB bulb calibrated not to exceed an intensity of 1000 W/m^2. Appendix A shows pyranometer readouts associated with each experiment. Light intensity was monitored with a pyranometer placed in the locus of highest light intensity.

The disinfection procedure was then run for four hours, sampling and plating both bottles in 100 µL aliquots every 30 minutes from the beginning of experimentation. At the conclusion of the experiment, the agar plates were placed into an incubation chamber set at 37º C for 24 hours. At the end of the incubation chamber, the number of CFU's on each plate was counted and photographed. These photographs are included in Appendix A and divided by experiment.

Table 2: Nanomaterials used during experimentation

Experiment #	Type of Nanomaterial Insert
Experiment 1	Pure TiO_2
Experiment 2	1.5% MoS_2- 98.5% TiO2
Experiment 3	5% MoS_2- 95% TiO2
Experiment 4	10% MoS_2- 90% TiO2
Experiment 5	No Insert utilized

Results and Discussion

The results of the disinfection experiments testing the efficiency of the MoS2-TiO2 nanomaterial are summarized in Tables 3 to 7.

Table 3: Graphic representation of agar plate counts, pure TiO_2.

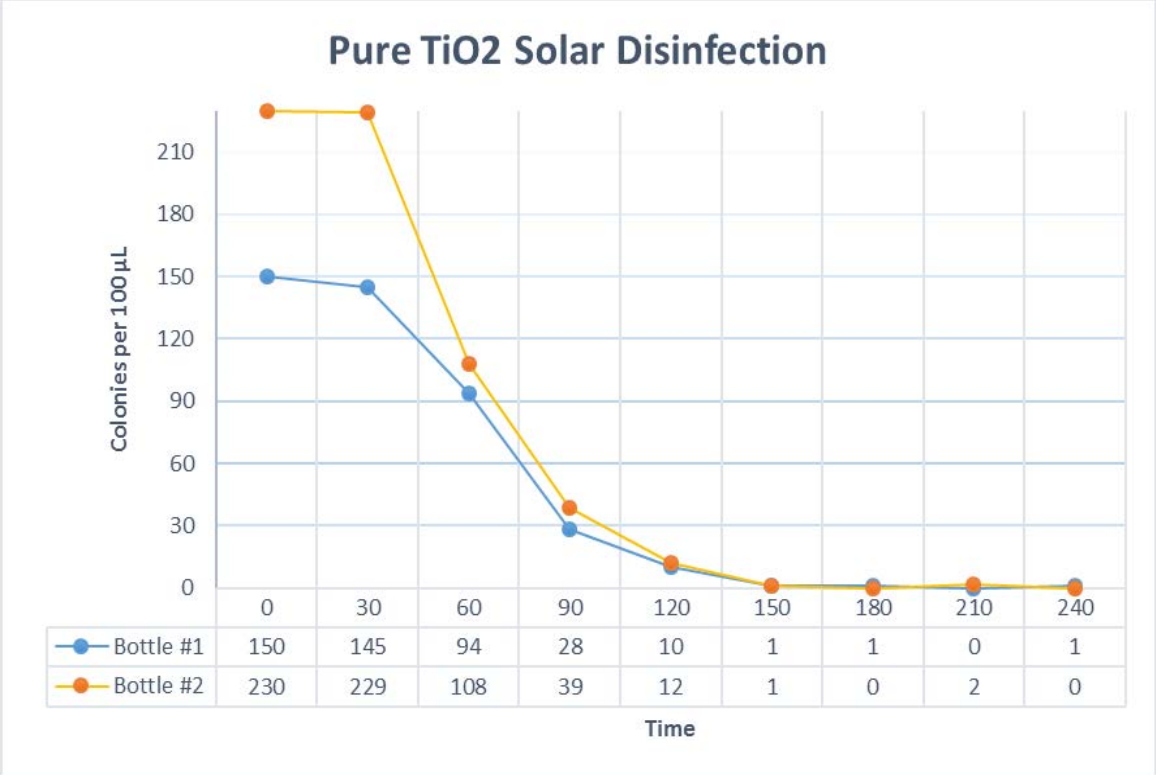

	0	30	60	90	120	150	180	210	240
Bottle #1	150	145	94	28	10	1	1	0	1
Bottle #2	230	229	108	39	12	1	0	2	0

Experiment 1: pure TiO_2 disinfection properties

The starting colony count for bottle #1 was 1500 CFU/ml, with bottle #2 at 2300 CFU/ml; these values were within the experimental goal range of 300 to 3000 CFU/ml. For both bottles, the timeframe of greatest colony decrease occurred between the 30 to 90-minute sampling periods (Tab. 3). Bottle #2 experienced the highest rate of disinfection during this time with an 81% decrease in viable CFU's between 30-90 minutes. By the 60-minute sampling time, both bottles displayed a similar level of

colonies (#1 940 CFU/ml, #2 1080 CFU/ml), despite Bottle #2 starting with a colony count 800 CFU/ml higher than bottle #1. The sample bottles continued this trend of similar colony counts through the remainder of the experiment, with both bottles reaching baseline (10 CFU/ml) by the 150-minute sampling mark. These results indicate that Bottle #1 went from a total number of bacteria around 1.5 million, and Bottle #2 a total of 2.3 million, to less than 10,000 bacteria per bottle within 150 minutes, demonstrating that pure TiO_2 inserts serve as an effective disinfection tool.

Table 4: Graphic representation of agar plate counts, 1.5% MoS_2-98.5% TiO_2.

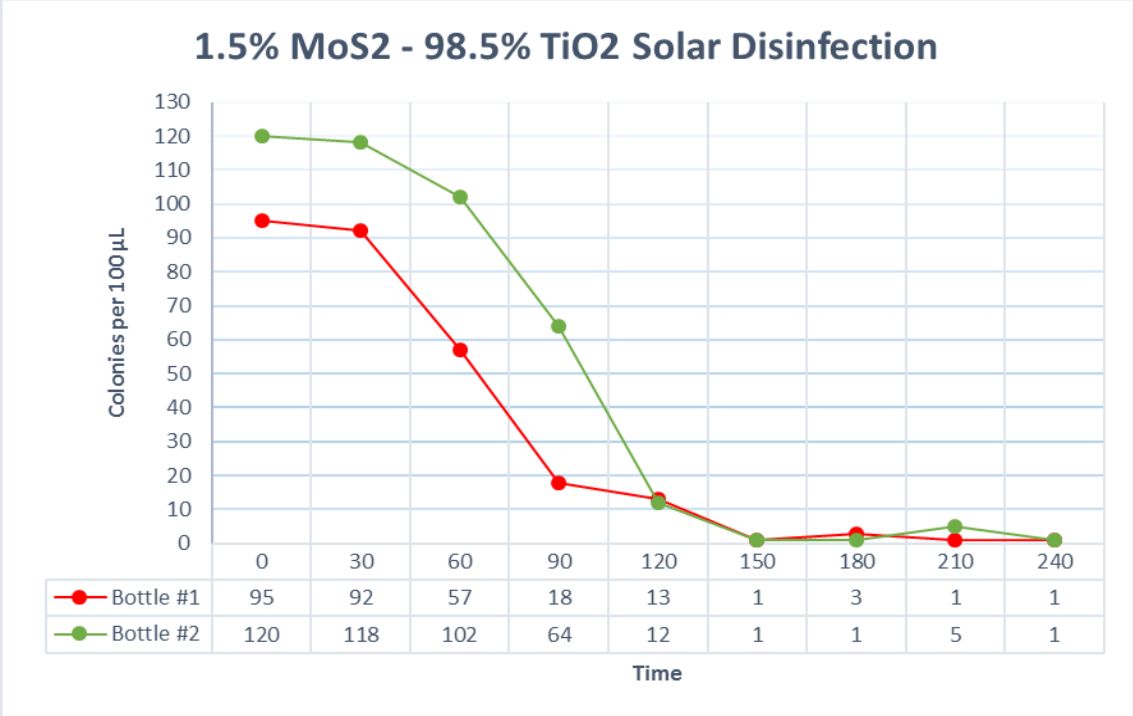

Experiment 2: 1.5% MoS_2-98.5% TiO_2 disinfection properties

Starting colony counts for this experiment were recorded at 950 CFU/ml for Bottle #1, and 1200 CFU/ml for Bottle #2. These counts were well within the desired experimental range. Bottle #1 decreased most significantly in viable bacteria

concentration between the 30 and 90-minute collection times, with an overall decrease of 80% viable CFU's during this period (Table 4). Comparatively, Bottle #2 decreased the most significantly between the 30 and 120-minute sampling window; a higher starting colony count likely led to this difference, with Bottle #2 starting 250 CFU/ml higher than Bottle #1. By 120 minutes both bottles contained a nearly equal number of CFU's (130 CFU/ml and 120 CFU/ml, respectively), despite differences in initial colony counts. Similar to the pure TiO_2 inserts, these inserts reached baseline by the 150-minute sampling period, with only 10 CFU/ml recorded per bottle.

Table 5: Graphic representation of agar plate counts, 5% MoS_2-95% TiO_2

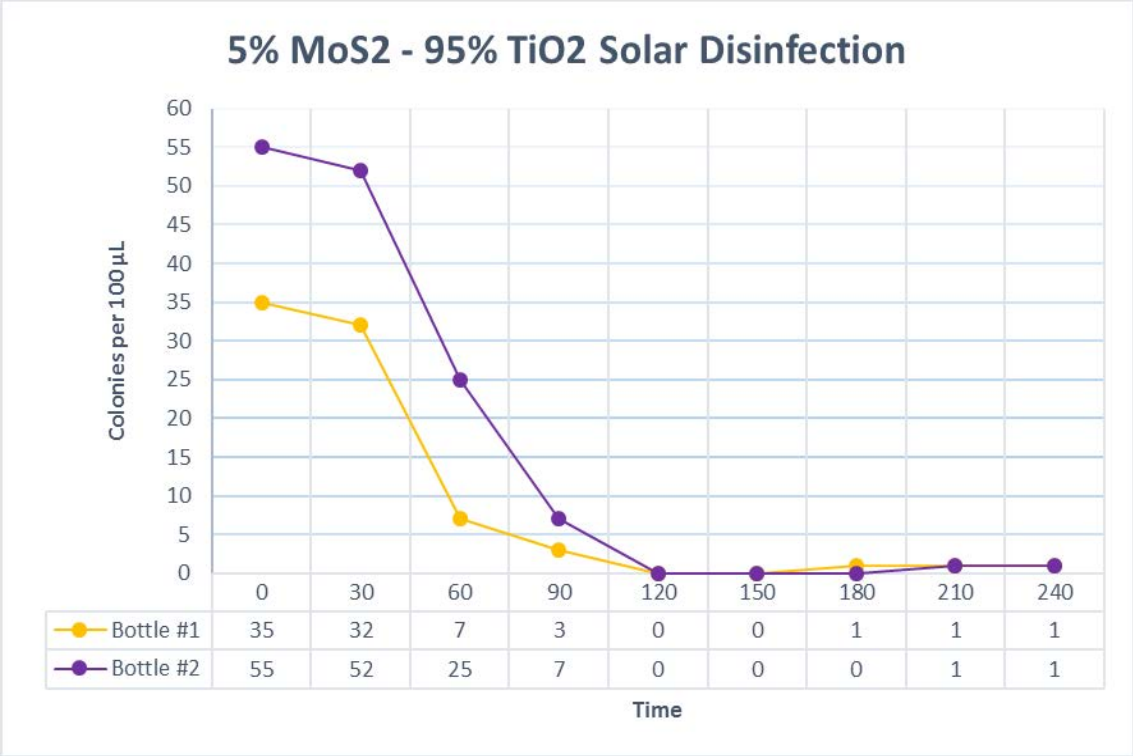

	0	30	60	90	120	150	180	210	240
Bottle #1	35	32	7	3	0	0	1	1	1
Bottle #2	55	52	25	7	0	0	0	1	1

Experiment 3: 5% MoS_2-95% TiO_2 disinfection properties

For experiment 3, a starting colony count of 350 CFU/ml was recorded for Bottle #1, and 550 CFU/ml for Bottle #2. Although this is a low starting colony count for Bottle #1, it was within target experimental starting colony ranges and thus qualifies as viable data. In addition, Bottle #2 starting at 550 CFU/ml was higher than other initial colony counts. Most importantly for comparison, this count was higher than both Bottles #1 (500 CFU/ml) and #2 (400 CFU/ml) for disinfection without an insert. Low colony count most likely resulted from reuse of leftover bacterial suspension in saline from a previous day's experimental trial. Lack of broth media in the saline suspension resulted in inactivation of a portion of the E. coli, thus yielding a lowered starting concentration when utilized.

Bottle #1 experienced the highest decrease in viable colonies between 30 and 60 minutes, with a 52% decrease between sampling windows (Table 5). In contrast, Bottle #2 experienced its greatest decrease in concentration between the 30 to 90 minute sampling times, dropping from 520 CFU/ml to 70 CFU/ml. By 90 minutes, Bottle #1 registered a colony count of 30 CFU/ml, with Bottle #2 at 70 CFU/ml. Comparatively, it took the bottles with no insert 60 minutes longer (150-minute sampling window) to reach the same levels of E. coli inactivation. By the 120-minute mark, both bottles reached a viable colony count of 0, with no rebound afterwards. This was the only experimental treatment which was completely disinfected by the 120-minute sampling window. Although these results indicate that 5% MoS_2-95% TiO_2 nanomaterial disinfected the water samples more quickly than any other insert, it should be noted that this experiment had the lowest initial colony forming unit counts of all experiments that made use of the nanomaterial inserts.

Table 6: Graphic representation of agar plate counts, 10% MoS_2- 90% TiO_2.

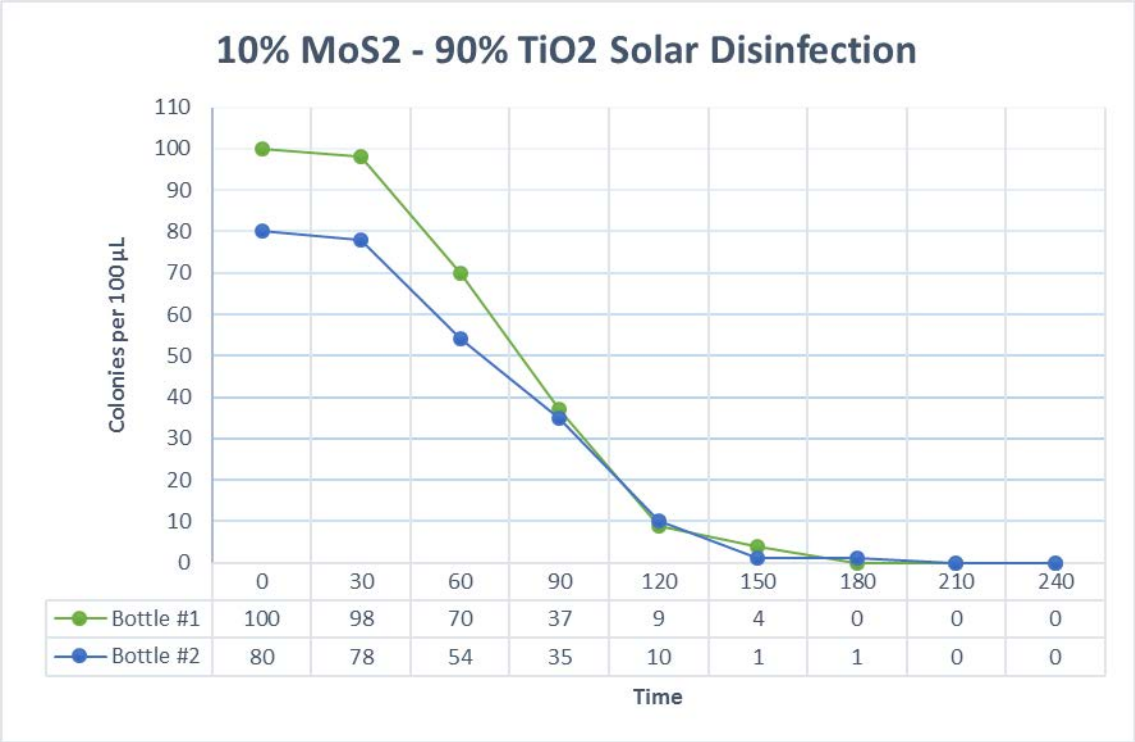

	0	30	60	90	120	150	180	210	240
Bottle #1	100	98	70	37	9	4	0	0	0
Bottle #2	80	78	54	35	10	1	1	0	0

Experiment 4: 10% MoS_2-90% TiO_2 disinfection properties

For the experiment with the highest concentration molybdenum disulfide nanomaterial inserts, starting colony counts were recorded at 1000 CFU/ml for Bottle #1, and 800 CFU/ml for Bottle #2. These counts were well within the 300 to 3000 CFU/ml desired range. Both bottles displayed the greatest decreases in concentration between the 30-minute and 120-minute sampling periods (Table 6). Bottle #1 demonstrated a 90% reduction in viable colonies between these time periods, and Bottle #2 registered an 87% reduction within the same time. By 120 minutes, total viable CFU's had dropped down to 90 CFU/ml and 100 CFU/ml for Bottles #1 and #2, respectively. This aligns closely with colony counts for the pure TiO_2 inserts at the 120-minute sampling time, which registered

100 CFU/ml for Bottle #1 and 120 CFU/ml for Bottle #2. This comparison illustrates that at a 10% concentration, the increased absorption potential of MoS_2 did not enhance the potential of the TiO_2 particles to inactivate E. coli beyond what it could in a pure state. Similar to the disinfection properties of 1.5% MoS_2-98.5% TiO_2 and the pure TiO2 inserts, near complete inactivation of bacteria occurred at the 150-minute mark. This demonstrates no improvement against the pure TiO_2 control but still yield more effective results than disinfection mediated without the use of nanomaterial inserts.

Table 7: Graph representation of plate counts, no insert.

	0	30	60	90	120	150	180	210	240
Bottle #1	40	37	9	1	7	5	0	5	1
Bottle #2	50	50	50	23	5	2	0	0	2

Experiment 5: no insert disinfection properties

For the fifth experiment, no insert or nanomaterial was utilized. This experiment was intended to illustrate the disinfection potential of the most basic model of the solar disinfection platform and essentially served as a control. Bottle #1 had a recorded starting

colony count of 400 CFU/ml, with Bottle #2 registering at 500 CFU/ml. Both of these starting counts were within desired experimental ranges. Bottle #1 dropped significantly between the 30- to 90-minute sampling windows, from 370 CFU/ml all the way down to 10 CFU/ml (Table 7). This low colony count may have been anomalous, as an increase in total colonies was recorded in the sampling period immediately afterwards, with 70 CFU/ml at the 120-minute sampling period. In comparison, Bottle #2 did not register a decrease in colony counts until after the 60-minute sampling time. Between 60 and 120 minutes Bottle #2 decreased in viable colonies from 50 down to 5, which represents a 90% decrease. Full disinfection was recorded at 180 minutes, with both bottles recorded at a 0-colony count at this sampling time. Despite results at the three-hour mark, results were contraindicated by a high plate count of 50 CFU/ml at the 210-minute mark for Bottle #1. These results could demonstrate that viable bacteria still remained after the 180 minute-period or they may simply be due to analytical error. These results serve to illustrate the photocatalytic potential of nanomaterials containing TiO_2.

Table 8: Summary of percent decrease in bacterial count by time period

T - T+30	30-60 minutes	60-90 minutes	90-120 minutes	120-150 minutes	Time to baseline (0 colony count)
Pure TiO2	45%	67%	67%	91%	150 minutes
1.5% MoS_2-98.5% TiO_2	26%	53%	55%	92%	150 minutes
5% MoS_2-95% TiO_2	65%	65%	100%	-	120 minutes
10% MoS_2-90% TiO_2	30%	41%	14%	73%	150 minutes
No Insert	38%	72%	339% (increase)	45%	240 + minutes

The percent decrease for each time period was calculated as: $Z\ \% =$

$$\frac{1}{2}\left[\frac{Abs\left(N_{1(T)}-N_{1(T+30)}\right)}{N_{1(T)}}+\ \frac{Abs\left(N_{2(T)}-N_{2(T+30)}\right)}{N_{2(T)}}\right]*100$$

Where N_1=bottle #1 CFU/100 µL, N_2= bottle #2 CFU/100 µL and T= time of sample collection

Discussion:

This project was undertaken with the goals of successfully synthesizing a variety of MoS_2-TiO_2 blends, quantitatively and qualitatively analyzing their properties, and integrating these nanomaterial blends into an inexpensive disinfection platform. A key facet of this project was to improve upon the photocatalytic potential of pure TiO_2 by increasing absorption in the UVA/UVB regions and into the visible region through doping with MoS_2, and to then utilize this improvement to decrease disinfection time in the Solar Disinfection (SODIS) platform. It was hypothesized that a particular blend of

MoS_2-TiO_2 nanomaterial would be more effective in disinfection while integrated into the SODIS platform when compared to pure TiO_2 nanomaterial.

Results from the characterization phase of the project leaned on the assumption that 1.5% MoS_2-98.5% TiO_2 would be the most effective nanomaterial blend. This assumption stemmed from three sources. First, the XRD measurements indicated that the 1.5% MoS_2 nanomaterial was the only blend which successfully integrated MoS_2 molecules without compromising TiO_2, being the highest intensity peaks in the readout (Figure 5). Second, FTIR analysis indicated that from 420-500 cm^{-1} the 1.5% MoS_2 blend had the lowest percent transmission besides the pure MoS_2 sample, as well as the greatest reduction in percent transmission relative to percent MoS_2 utilized during synthesis (Figure 9). Third, UV-Vis measurement indicated an increase in absorption in the 280-400 cm^{-1} range, which constitutes UVA and UVB light (Fig. 8). 1.5% MoS_2-98.5% TiO_2 was enhanced in absorption through 350-380 cm^{-1} to the same level as 5% MoS_2-95% TiO_2, without the potential interference posed by an increased concentration of MoS_2.

Despite the hypothesis that 1.5% MoS_2-98.5% TiO_2 would be the most effective nanomaterial blend when integrated into the SODIS platform, this was not the case. Applicatory testing of the nanomaterials in comparison to pure TiO_2 and unassisted SODIS revealed that 1.5% MoS_2-98.5% TiO_2 was no more effective than pure TiO_2 within the given sampling timeframe, although all nanomaterial blends disinfected more quickly than SODIS without the assistance of nanomaterial inserts (Table 6). The only blend which appeared to disinfect more quickly than pure TiO2 was that of the 5% MoS_2-95% TiO_2 blend (Table 5). This particular blend appeared to reduce the total time required for disinfection from 150 minutes down to 120 minutes. Although this result

appears promising, it could be caused by a lower starting concentration of E. coli. The 5% MoS_2-95% TiO_2 experiment started at 350 CFU/ml and 550 CFU/ml for Bottles #1 and #2, respectively (Table 5). If bacterial concentration had been doubled or tripled, confirmatory results would have been easier to assess when compared to the other nanomaterial blends.

Potential reasons for the 5% MoS_2-95% TiO_2 blend outperforming the other blends could be derived from the difficulty of finely milling materials which contain MoS_2. MoS_2 has a key application as a solid state industrial lubricant with antifriction properties (Windom et al., 2011). As evidenced by the SEM readings, milling became less effective as concentration of MoS_2 increased, with 10% MoS_2-90% TiO_2 demonstrating the lowest improvement post-milling (Figures 16,17). If this is correct, the 5% MoS_2 batch would have benefitted from smaller particle size compared to 10% MoS_2 batch, with decreases in particle size generally correlated to increased photocatalytic activity (Amano et al., 2013). A reason why 5% MoS_2-95% TiO_2 outperformed the 1.5%-98.5% nanomaterial blend could stem from an increased absorption potential offered by the MoS_2 in the UVA/UVB wavelengths, at a similar level of milling (Fig. 8).

A primary consideration to take into account should be the cost of MoS_2-TiO_2 nanomaterial blends in relation to pure TiO_2. A key goal of this project was to develop a cost-effective method of solar disinfection. Currently, there is no commercial source for any of the synthesized MoS_2-TiO_2 nanomaterial blends tested by this project. The Sol-Gel procedure utilized for generation of the MoS_2-TiO_2 nanomaterials makes use of relatively expensive precursor material including titanium isopropoxide and the MoS_2 itself. It is also labor intensive and requires a skilled chemist to properly manufacture. As

an alternative, bulk TiO2 nanomaterial is available from generic chemical distributors for roughly $11/kilogram. Thus, despite the potential 30-minute reduction in disinfection time offered by the 5% MoS_2-TiO_2 blend, far more inserts could be manufactured for the same amount of money and time invested into their production. Pure TiO_2 inserts are therefore far more economical and efficient to develop for practical applications. In addition to this, the use of black silicone on the SODIS inserts could impart pure TiO_2 with increased absorption potential without the need to generate a complex nanomaterial blend. If research into this subject was continued, this would be a key variable to continue testing. On the other hand, this study was preliminary in nature and the fact that the 5% MoS_2-TiO_2 blend outperformed even pure TiO_2 may be cause for more detailed research to determine conclusively if this is the case. If these results hold, then alternative methods to lower the costs of production might be merited.

Chapter 4: Conclusions

This project successfully demonstrated that a variety of nanomaterial blends can be generated between MoS_2 and TiO_2 with their own unique chemical properties. These materials were then characterized utilizing advanced methods including XRD, SEM, UV-VIS, and FTIR with results outlined in chapter 2. Finally, all of these blends were demonstrated to be more effective than traditional solar disinfection mediated without the use of nanomaterial.

The results of studies to determine the effectiveness of each blend at disinfecting water indicate that the 5% MoS_2-95% TiO_2 blend yielded the best results, indicating superior photocatalytic potential compared to pure TiO_2. This suggests that there may be an optimum blend – the 1.5% MoS_2-95% TiO_2 blend may not have enough dopant to enhance the photocatalytic properties of TiO_2 and the 10% MoS_2-95% TiO_2 blend may have too much dopant which has a negative effect on those properties. The results from XRD analysis showed that the 1.5% MoS_2-95% TiO_2 blend's properties were dominated by the TiO_2 while the 10% MoS_2-95% TiO_2 blend's properties were dominated by the dopant. On the other hand, the properties of the 5% MoS_2-95% TiO_2 blend was a mixture of both compounds. This latter blend seems to be closer to the optimum blend. Further studies could elucidate this more clearly.

Chapter 5: References Cited

Amano, Fumiaki, Ishinaga, Eri and Akira Yamakata. “Effect of Particle Size on the Photocatalytic Activity of WO3 Particles for Water Oxidation”. *The Journal of Physical Chemistry*. (2013). 22584-22590.

Asahi, R, Morikawa, T, Aoki, K, and Y. Taga. "Visible-light photocatalysis in nitrogen-doped titanium oxides". *Science* 293.5528 (2001). 269-271.

Carp, O, Huisman, L, and A. Reller. "Photoinduced reactivity of titanium dioxide." *Progress in solid state chemistry* 32.1-2. (2004). 33-177.

Chen, Xiaobo, Shen, Shaoshua, Guo, Liejin and Samuel Mao. "Semiconductor-based photocatalytic hydrogen generation". *Chemical reviews* 110.11. (2010). 6503-6570.

Chenari, Hossein Mahmoudi, Seibel, Christoph, Hauschild, Dirk, Reinert, Friedrich, & Abdollahian, Hossein. “Titanium Dioxide Nanoparticles: Synthesis, X-Ray Line Analysis and Chemical Composition Study”. *Materials Research*, *19*(6). (2016). 1319-1323.

Clasen, Thomas and Laurence Haller. “Water Quality Interventions to Prevent Diarrhoea: Cost and Cost-Effectiveness”. *Public Health and the Environment*. World Health Organization Geneva. (2008). 1-33.

Diebold, U. "The surface science of titanium dioxide." *Surface Science Reports* 48.5-8. (2003). 53-229.

Emery, Keith. “*Reference Solar Spectral Irradiance: Air Mass 1.5*”. American Society for Testing and Materials (ASTM) Terrestrial Reference Spectra for Photovoltaic Performance Evaluation. (2002). 1-20.

Fahey, D.W., and M.I. Hegglin, Twenty Questions and Answers About the Ozone Layer: 2010 Update, Scientific Assessment of Ozone Depletion: World Meteorological Organization, Geneva, Switzerland. (2011). 1-72.

Fujishima, Akira and Kenichi Honda. “Electrochemical Photolysis of Water at a Semiconductor Electrode”. *Nature* 238. (1972). 27-38.

Forsberg, Viviane, et al. "Exfoliated MoS2 in Water without Additives." *PLoS One* 11.4. (2016). 1-12.

Gelover, Silvia, Gomez, Luis, Reyes, Karina and Teresa Leal. "A practical demonstration of water disinfection using TiO2 films and sunlight". *Water research* 40.17. (2006). 3274-3280.

Gunti, Srikanth, Michael McCrory, Ashok Kumar, and Manoj K. Ram. "Enhanced Photocatalytic Remediation Using Graphene (G)-Titanium Oxide (TiO2) Nanocomposite Material in Visible Light Radiation." *American Journal of Analytical Chemistry*. (2016). 576-587.

Hench, LL, JK K West. "The Sol-Gel Process." *Chemical reviews* 90.1. (1990). 33-72.

Hwu, Y.; Yao, Y. D.; Cheng, N. F.; Tung, C. Y.; Lin, H. M.X-ray absorption of nanocrystal TiO2. *Nanostructured Materials* Volume 9, Issues 1–8. (1997). 355-358.

Kun Hong Hu, Xian Guo Hu, Yu Fu Xu, Jia Dong Sun. "Synthesis of TiO2 nanocomposite and its catalytic degradation effect on methyl orange. *Journal of Materials Science*. Volume 45, Issue 10. (May 2010). 2640–2648.

Lee, Changgu, et al. "Frictional characteristics of atomically thin sheets." *Science* 328.5974. (2010).76-80.

Lonnen, J, Kilvington, S, Kehoe, S. C, Al-Touati, F, McGuigan, K. G. "Solar and photocatalytic disinfection of protozoan, fungal and bacterial microbes in drinking water". *Water research* 39.5. (2005). 877-883.

Luttrell, Tim, Halpegamage, Sandamali, Tao, Junguang, Kramer, Alan, Eli Sutter and Matthias Batzill. "Why is anatase a better photocatalyst than rutile? - Model studies on epitaxial TiO2 films". *Scientific Reports* 4, Article number: 4043. (2014). 33-76.

Matsumi, Yutaka, and Masahiro Kawasaki. "Photolysis of atmospheric ozone in the ultraviolet region." *Chemical reviews* 103.12. (2003). 4767-4782.

Meierhofer, Regula, Wegelin, Martin, Rosario-Torres, Xiomara, Gremion, Bruno, Mercado, Alvaro, Mäusezahl, Daniel, Hobbins, Michael, Indergand-Echeverria, Stephan, Beat Grimm and Christina Aristanti. "Solar Disinfection: A Guide for the Application of SODIS". Swiss Federal Institute of Environmental Science and Technology, Department of Water and Sanitation in Developing Countries. (2002). 1-80.

Odonkor, Stephen and Joseph Ampofo. "Escherichia coli as an indicator of bacteriological quality of water: an overview". Environmental Biology and Health Division, Water Research Institute, Ghana. *Microbiology Research 2013; volume 4:e2*. (2013). 1-7.

Sakurai, Kenji, and Mari Mizusawa. "X-ray diffraction imaging of anatase and rutile." *Analytical chemistry* 82.9 (2010). 3519-3522.

Sanchez, C, Julian, B, Belleville, P, and M. Popall. "Applications of hybrid organic-inorganic nanocomposites." Journal of materials chemistry 15.35-36. (2005). 3559-3592.

United States Environmental Protection Agency. "*UV Radiation*". EPA 430-F-10-025. (2010). https://www.epa.gov/sites/production/files/documents/uvradiation.pdf

United States Environmental Protection Agency, Office of Water. "The history of drinking water treatment". Fact Sheet EPA-816-F-00-006, United States. (2000). 1-4.

Wang C-C, Zhang Z, Ying JY. "Photocatalytic decomposition of halogenated organics over nanocrystalline titania". *Nanostructured Materials.* (1997). 583–586.

Windom, B.C., Sawyer, W.G. & Hahn, D.W. "A Raman Spectroscopic Study of MoS_2 and MoO_3: Applications to Tribological Systems". *Tribology Letters*. (2011). 301-310.

Zhang, Weiping, Xiao, Xinyan, Zhang, Lili, and Caixia Wan. "Fabrication of TiO2 Composite Photocatalyst and Its Photocatalytic Mechanism for Degradation of Methyl Orange under Visible Light". *The Canadian journal of chemical engineering* 93.9. (2015). 1594-1602.

Zongyou Yin, Hai Li, Hong Li, Lin Jiang, Yumeng Shi, Yinghui Sun, Gang Lu, Qing Zhang, Xiaodong Chen, and Hua Zhang. "Single-Layer MoS2 Phototransistors". ACS *Nano 6* (1). (2012). 74-80.

Appendix A

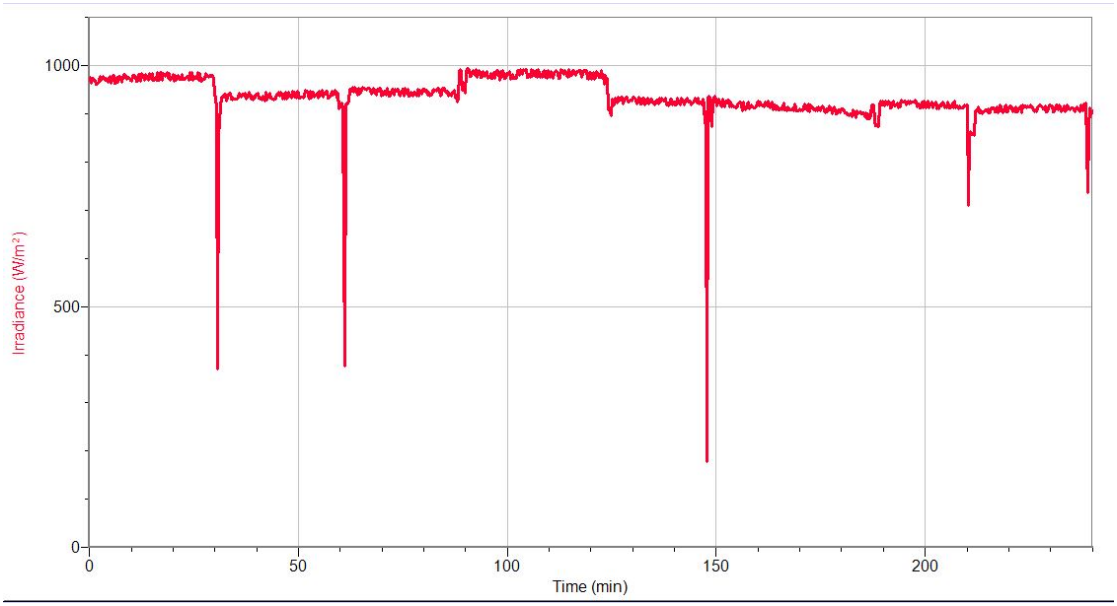

Figure A1: Pyranometer readout, pure TiO_2

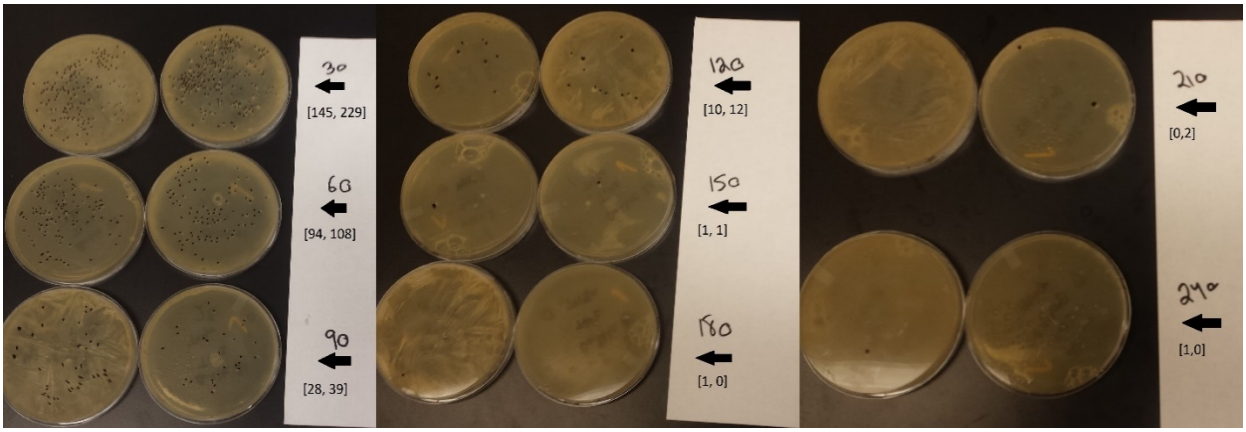

Figure A2: Agar plate counts, pure TiO_2

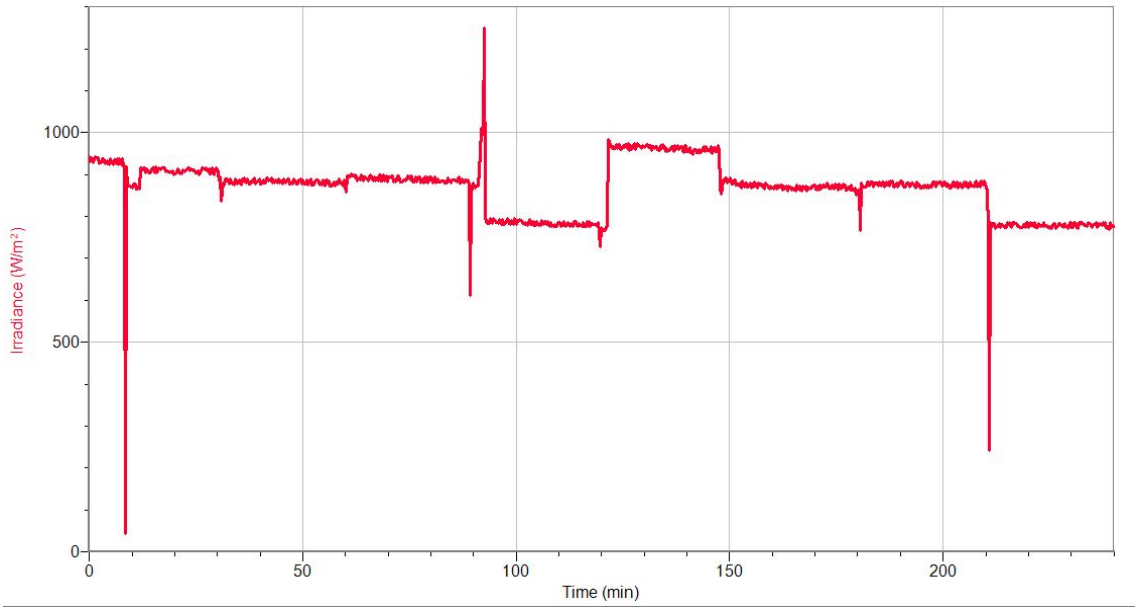

Figure A3: Pyranometer readout, 1.5% MoS_2-98.5% TiO_2

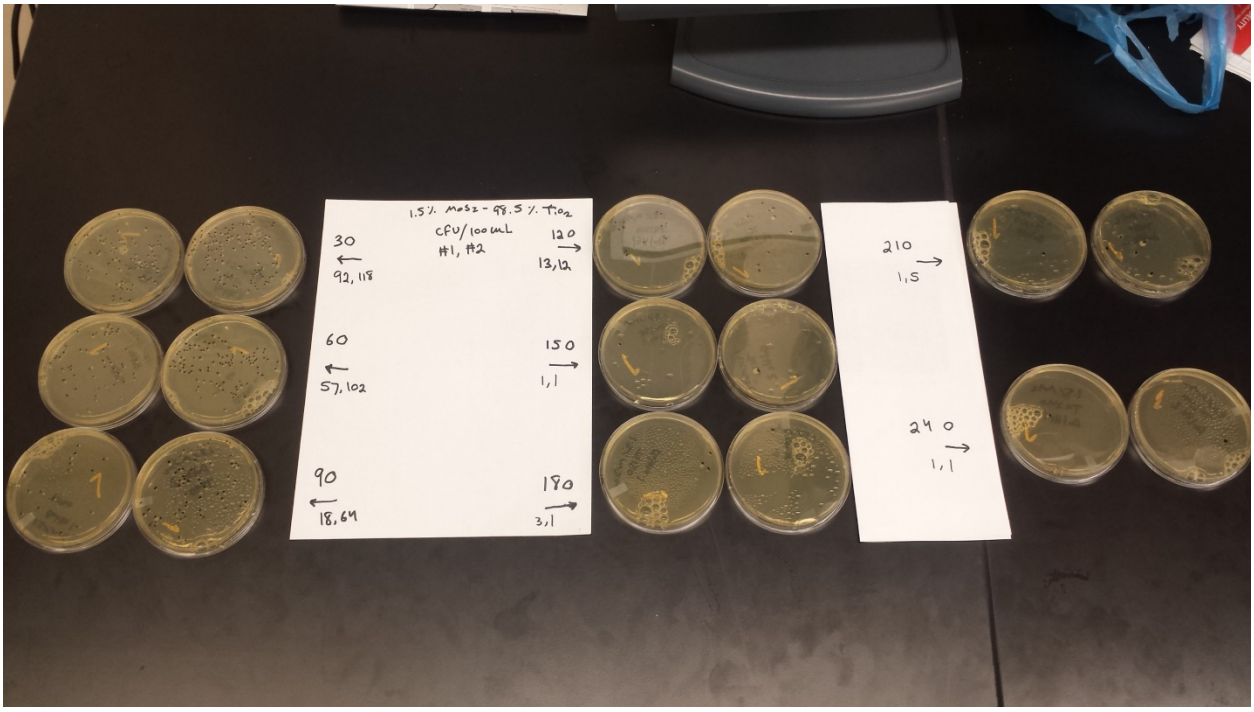

Figure A4: Agar plate counts, 1.5% MoS_2- 98.5% TiO_2

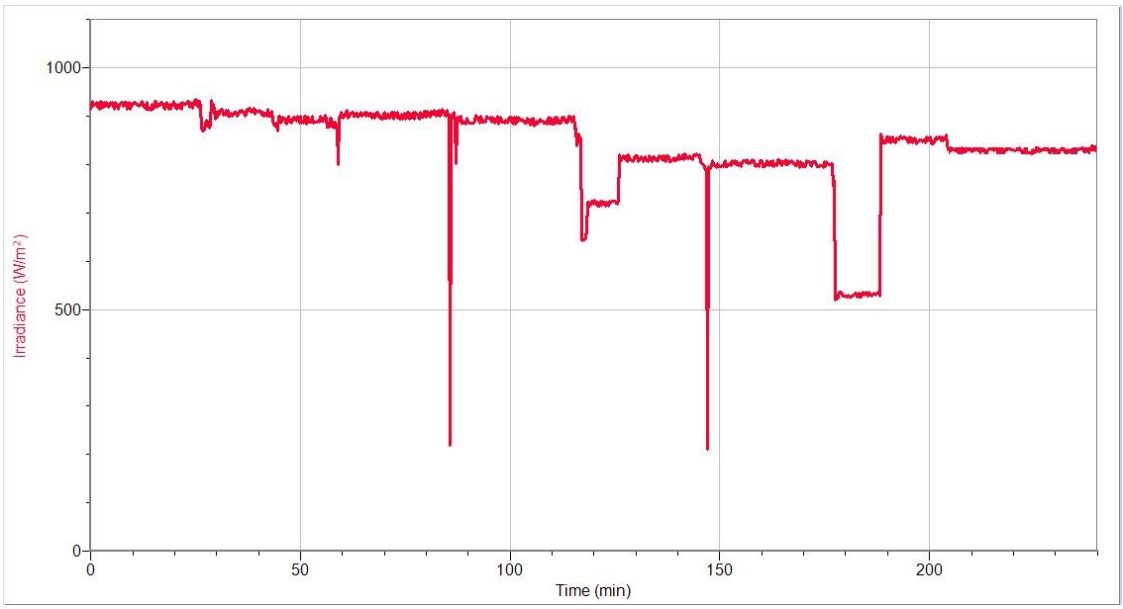

Figure A5: Pyranometer readout, 5% MoS_2-95% TiO_2

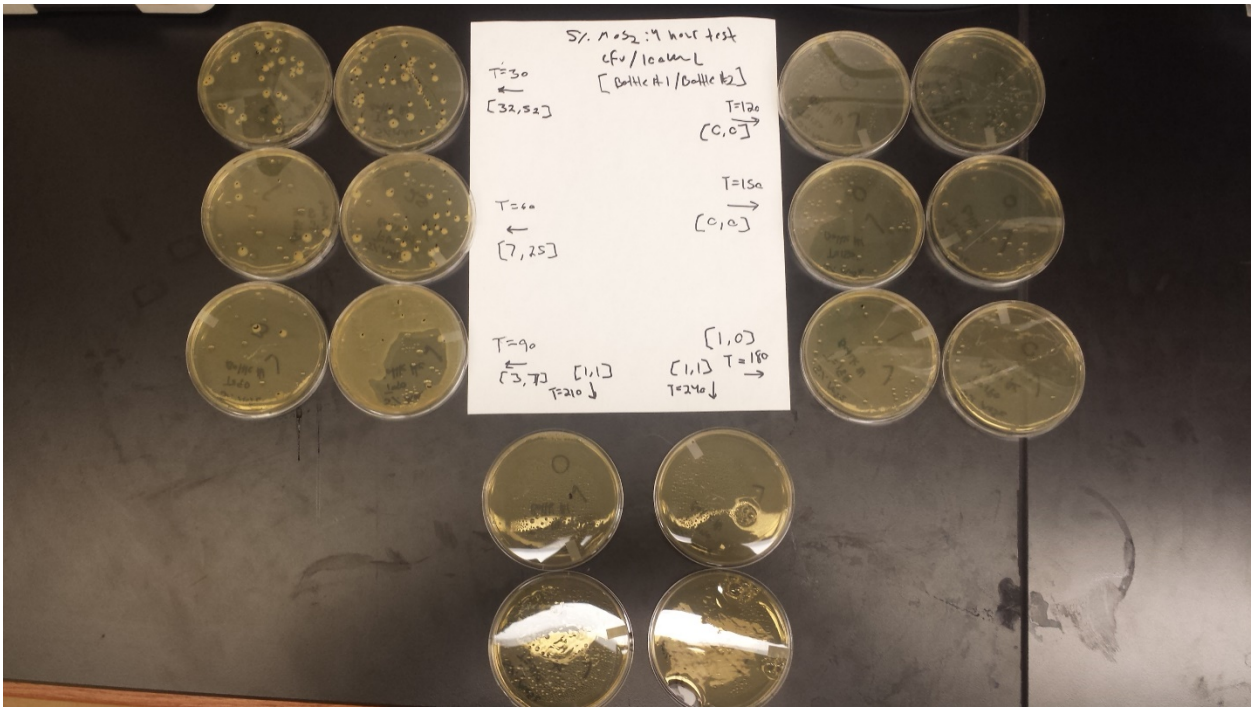

Figure A6: Agar plate counts, 5% MoS_2-95% TiO_2

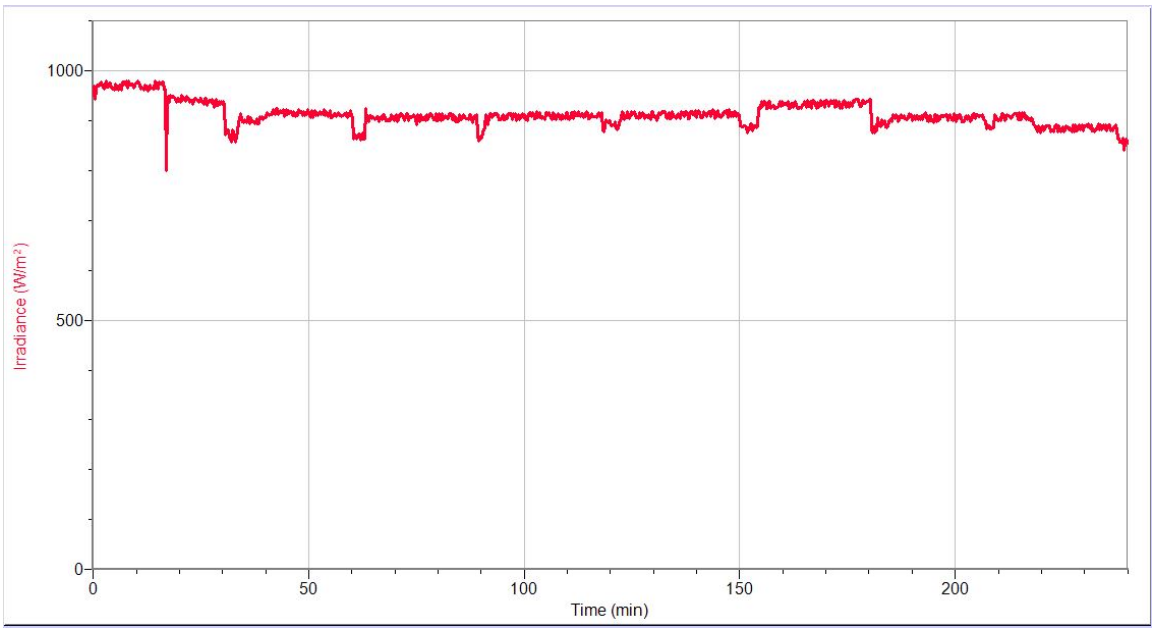

Figure A7: Pyranometer readout, 10% MoS_2- 90% TiO_2

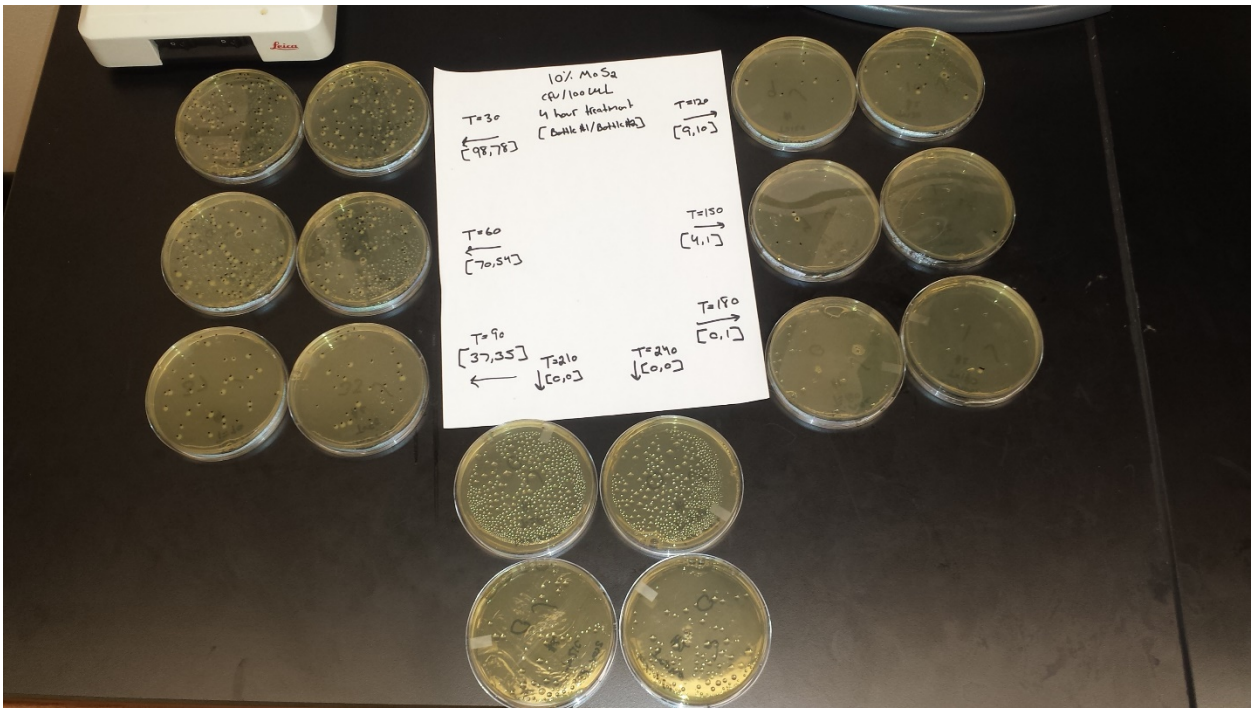

Figure A8: Agar plate counts, 10% MoS_2- 90% TiO_2

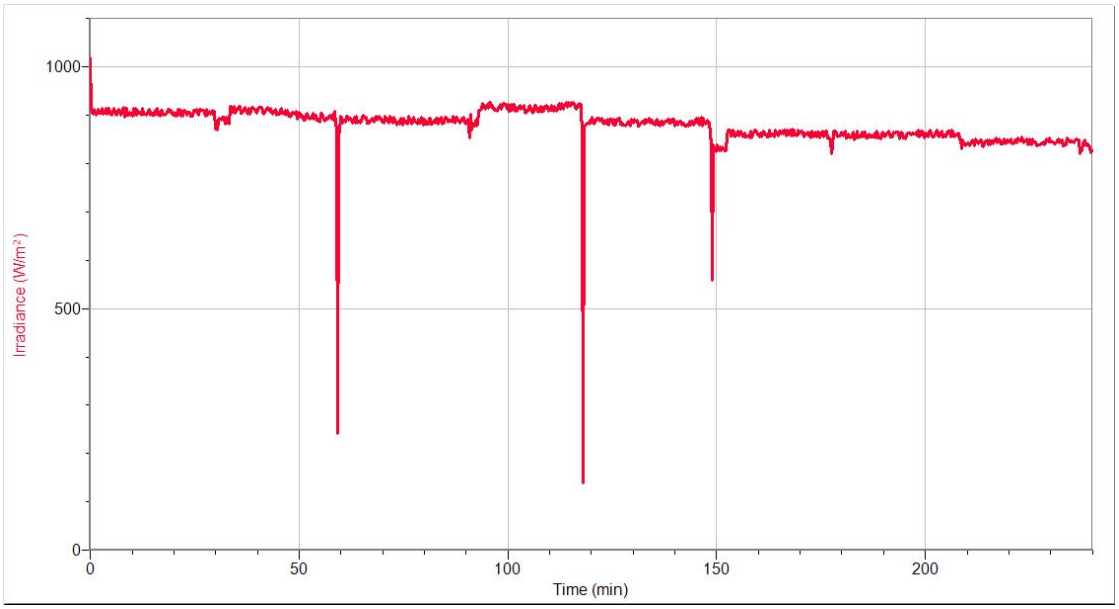

Figure A9: Pyranometer readout, no insert

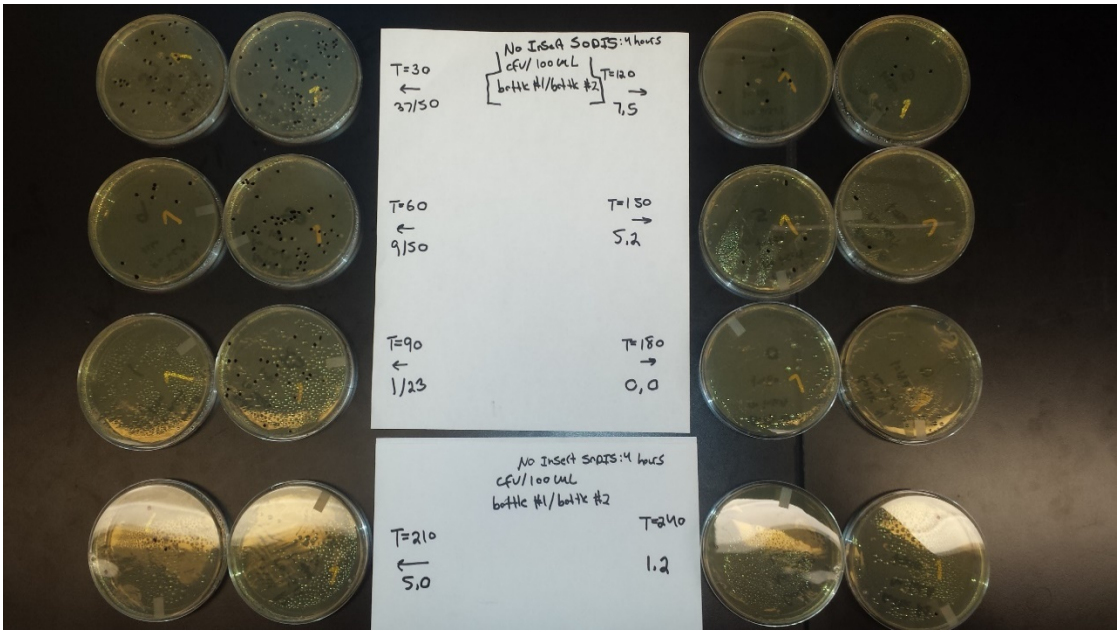

Figure A10: Agar plate counts, no insert